1972-03

An investigation of linear transients associated with a time dependent bottom spiral

Camp, Norman Thomas

http://hdl.handle.net/10945/16207

AN INVESTIGATION OF LINEAR TRANSIENTS ASSOCIATED WITH A TIME DEPENDENT BOTTOM SPIRAL

Norman Thomas Camp

NAVAL POSTGRADUATE SCHOOL

Monterey, California

THESIS

AN INVESTIGATION OF LINEAR TRANSIENTS ASSOCIATED WITH A TIME DEPENDENT BOTTOM SPIRAL

by

Norman Thomas Camp

Thesis Advisor: J.A. Galt

March 1972

An Investigation of Linear Transients Associated With a Time Dependent Bottom Spiral

by

Norman Thomas Camp
Lieutenant Commander, United States Navy
Ed.B., Rhode Island College, 1962

Submitted in Partial fulfillment of the
requirements for the degree of

MASTER OF SCIENCE IN OCEANOGRAPHY

from the

NAVAL POSTGRADUATE SCHOOL
March 1972

ABSTRACT

Ekman's linear equations for time dependent flow (neglecting wind stress) are solved using a time dependent Green's function and the method suggested by Welander (1957). The solution represents the vertical velocity profile in terms of the local time history of the changes in sea surface elevation determined by the divergence of the flow in the vertically integrated continuity equation.

A fully implicit finite-difference scheme is developed to represent a time dependent seiche oscillating across a shallow infinite channel. The transients associated with the formation of the bottom spiral are clearly represented by the model and the influence of friction and Coriolis are individually and collectively introduced. The model allows independent calculation of velocity, volume transport, sea surface elevation, bottom stress, and the total energy balance of the system. The numerical scheme provides a method for adequately describing and investigating certain classes of time dependent motion, and its development suggests a mechanism for improving numerical prediction of storm surge.

TABLE OF CONTENTS

LIST OF TABLES

LIST OF FIGURES

ACKNOWLEDGEMENTS

The topic for this thesis was suggested by Assistant Professor Jerry A. Galt of the Naval Postgraduate School, Monterey, California. His valuable experience in the field of ocean dynamics and his guidance in developing the conceptual model contributed greatly to the successful completion of this research. Assistant Professor R.H. Franke provided helpful ideas during the research and contributed valuable time and thought reading the manuscript. To these people the author expresses his sincere thanks. Additionally the author wishes to express his long overdue appreciation to his wife, who provided a needed source of encouragement and a sympathetic ear.

I. INTRODUCTION

"The purpose of computing is insight not numbers"
(Hamming, 1962)

A. BACKGROUND

Oceanographers use a number of techniques for the study of oceanic flow including analysis of hydrographic data, use of hydraulic laboratory models, and mathematical treatment of the basic equations of motion. Initially oceanic circulation was treated as a steady state problem, and various investigators have been successful in representing and explaining many of the gross features of oceanic circulation using each of these techniques.

Mathematical treatment of oceanic circulation began with Ekman's analysis (1905) of wind-driven circulation and his results have been extended by a number of authors. (Sverdrup, 1947, Munk, 1950, Bryan, 1959) For the most part the study of large scale ocean dynamics has been done with steady state formulations.

Mathematical treatment of time dependent motion is far less complete in the literature than that of steady state. It is also far more difficult to compare results due to the scarcity of reliable data. The complex nature of the solutions to time dependent boundary value problems further increases this difficulty. These solutions take the form of varying differential, integral, and infinite series equations whose numerical evaluation was not feasible until the advent of the high speed computer and the development of appropriate numerical techniques.

In the last decade these methods have been applied, through numerical models, to the problems of explaining and predicting the various details of fluid motion in both the atmosphere and the oceans. Although much success has been attained with these methods, many critical questions still need explanation. Many of these questions relate to the structure of the various frictional boundary layers, the details of their development, and the resulting effects on the interior flow.

Many complicated engineering problems occur in near shore and other shallow water regions. The time dependent nature of these areas is well documented and the resulting flow is greatly modified due to interaction with the ocean bottom. Therefore an understanding of the nature of time dependent flow at all levels is fundamental to dealing with problems in these areas. The question of how readjustment takes place and how the many transients can be appropriately represented in the bottom frictional boundary layer has not been adequately explained. Further, it is necessary to understand the dynamic coupling between the flow and the development of the bottom boundary layer before accurate modeling techniques can be developed. It is towards this understanding that this work was directed.

B. PREVIOUS RELATED RESEARCH

Work by Welander (1957) dealt with obtaining time dependent solutions using Ekman dynamics. His results were presented in terms of a time dependent Green's function and were related to the problems of predicting tides and storm surges. He demonstrated that the velocity profile, volume transport, sea level elevation, and bottom stress could be exactly represented by his

"integro-differential" solution. It was suggested that this solution could be used to improve storm surge and tide predictions. A step-by-step numerical scheme was proposed, but the details of the scheme were not presented in the literature.

Galt (1970) covered much of the same material that Welander presented but used a different method of solution. The solution allowed a more explicit formulation of results which provided more insight into the possible transients present and the relevant time scales of each. He discussed the need for information relating to time dependent flow in shallow water regions, and suggested that the numerical investigation of the interaction between a seiche and its associated transient bottom spiral might be useful in determining how the various transients present are effectively coupled.

C. THESIS OBJECTIVES

Since the major area of interest was to be the bottom boundary layer, the first objective was to formally solve the governing equations neglecting wind stress. The solution would therefore not allow a surface Ekman spiral to develop and effect the interior flow. It will be showed that the solution can be represented by two equations, one integral and one differential. These equations are similar in form to the ones developed by Welander and Galt. Although both of these authors proposed that these equations could be solved numerically using step-by-step procedures, it was not initially apparent whether a stable and accurate numerical scheme was feasible. Therefore the second objective was to formulate a numerical model capable of simultaneously solving these equations.

Finally, as suggested by Galt, this model would be applied to represent a seiche to examine the relationships which developed between the various transients.

II. THE FORMAL SOLUTION

A. GOVERNING EQUATIONS AND ASSUMPTIONS

The momentum equations considered are essentially those used by Ekman. The non-linear and horizontal friction terms are assumed small and neglected. The Coriolis parameter, the density, and the coefficient of vertical friction are all assumed constant. Thus:

$$\frac{\partial u}{\partial t} - fv - k\frac{\partial^2 u}{\partial z^2} = -g\frac{\partial \xi}{\partial x} \qquad (1)$$

$$\frac{\partial v}{\partial t} + fu - k\frac{\partial^2 v}{\partial z^2} = -g\frac{\partial \xi}{\partial y}\ . \qquad (2)$$

Where u and v are velocities in the x and y-directions, f the Coriolis parameter, g the acceleration of gravity, and k the constant coefficient of vertical friction. $\xi(x,y,t)$ is the elevation of the free surface and the z-axis is considered positive up.

The third equation necessary to solve for u, v, and ξ is the vertically integrated continuity equation.

$$\frac{\partial \xi}{\partial t} + \frac{\partial U}{\partial x} + \frac{\partial V}{\partial y} = 0 \qquad (3)$$

where

$$U = \int_{-h}^{0} u\ dz \quad ; \quad V = \int_{-h}^{0} v\ dz \qquad (4)$$

is the volume transport and h = h(x,y) is the depth of the water. ξ is assumed small compared to h.

Neglecting the effects of wind stress on the motion results in the following linearized boundary conditions on u and v:

$$\left(\frac{\partial u}{\partial z}\right)_{z=0} = 0 \quad ; \quad \left(\frac{\partial v}{\partial z}\right)_{z=0} = 0 \tag{5}$$

$$(u)_{x=-h} = 0 \quad ; \quad (v)_{z=-h} = 0 \ . \tag{6}$$

For this development it was assumed that initially a state of rest exists:

$$(u)_{t=0} = 0 \quad ; \quad (v)_{t=0} = 0 \ . \tag{7}$$

As in Welander's work the following complex notation was introduced:

$$\begin{gathered} w = u + iv \\ \frac{\partial \xi}{\partial n} = \frac{\partial \xi}{\partial x} + i \frac{\partial \xi}{\partial y} \end{gathered} \tag{8}$$

Where $i = \sqrt{-1}$. Using this notation eqs. (1), (2), (6), and (7) can be expressed as follows:

$$\frac{\partial w}{\partial t} - k \frac{\partial^2 w}{\partial z^2} + ifw = - g \frac{\partial \xi}{\partial n} \tag{9}$$

$$\left(\frac{\partial w}{\partial z}\right)_{z=0} = 0 \tag{10}$$

$$(w)_{t=0} = 0 \tag{11}$$

$$(w)_{z=-h} = 0 \ . \tag{12}$$

Equations (9) through (12) define the initial/boundary valued problem that must be solved to specify u and v. Although $\left(\frac{\partial \xi}{\partial n}\right)$ in eq. (9) is not externally specified it can theoretically be determined by integrating eq. (3). This makes it possible to treat it as a time dependent forcing term (i.e. $\frac{\partial \xi}{\partial n}(t)$).

B. METHOD OF SOLUTION

To solve the problem begin by multiplying eqs. (9) through (12) by e^{ift} and introducing the relation $w^* = we^{ift}$. Then eqs. (9) through (12) can be written as:

$$\frac{\partial w^*}{\partial t} - k \frac{\partial^2 w^*}{\partial z^2} = - ge^{ift} \frac{\partial \xi}{\partial n} (t) \tag{13}$$

$$\left(\frac{\partial w^*}{\partial z}\right)_{z=0} = 0 \tag{14}$$

$$(w^*)_{t=0} = 0 \tag{15}$$

$$(w^*)_{z=-h} = 0 \; . \tag{16}$$

A solution to eqs. (13) through (16) can be obtained by using a time dependent Green's function approach as described below.

Assume

$$w^* = \phi_m(t) \; Z_m(z) \tag{17}$$

where $Z_m(z)$ satisfies the boundary conditions and $\phi_m(t)$ satisfies the initial conditions. $Z_m(z)$ is the eigen-function determined by applying standard separation of variables to the homogeneous part of eq. (13) using eqs. (14) and (16). It is found to be:

$$Z_m(z) = \cos(pz) \tag{18}$$

where

$$p = \frac{(2m-1)}{2} \frac{\pi}{h} \tag{19}$$

$\phi_m(t)$ is determined by substituting eq. (17) into eq. (13) requiring that $\phi_m(t)$ satisfy eq. (15), and using the orthogonality of the cosine function to determine the appropriate constants. Thus

$$\phi_m(t) = \frac{2g(-1)^m}{ph} \int_0^t e^{-kp^2(t-t')} e^{-ift'} \frac{\partial \xi}{\partial n}(t') dt' \; . \tag{20}$$

Therefore a solution to eqs. (13) through (16) is

$$w^{*}(x,y,z,t) = \frac{2g}{h}\sum_{m=1}^{\infty} \frac{(-1)^m \cos(pz)}{p} \int_0^t e^{-kp^2(t-t')} e^{-ift'} \frac{\partial \xi}{\partial n}(t')dt' \quad (21)$$

For the general time dependent solution of eq. (9), dividing eq. (21) by e^{ift} yields:

$$w(x,y,z,t) = \frac{2g}{h}\sum_{m=1}^{\infty} \frac{(-1)^m \cos(pz)}{p} \int_0^t e^{-(kp^2+if)(t-t')} \frac{\partial \xi}{\partial n}(t')dt' \quad (22)$$

C. DISCUSSION OF THE FORMAL SOLUTION

It is apparent at a glance that eq. (22) satisfies the boundary and initial conditions. Substituting eq. (22) into eq. (9) yields as a residue:

$$\sum_{m=1}^{\infty} \frac{(-1)^m}{ph} \cos(pz) = -1 \ . \quad (23)$$

It is easily verified that the left hand side of eq. (23) is simply the cosine expansion of the right hand side, and therefore eq. (22), in the limit, is an exact solution to the initial problem.

Equation (22) represents the horizontal currents at all depths resulting from the pressure gradient produced by the slope of the sea surface at a particular point and instant in time. The integral term carries a running summation of the currents resulting from the slope in the past history of the flow. These currents are modified in time by a rotation and decay represented by the weighting function

$$e^{-(kp^2+if)(t-t')}.$$

This weighting function introduces two interesting time scales into the problem. The first is the inertial rotation period, which

varies as a function of latitude. For mid-latitude locations it is on the order of 20 hours. The second time scale is introduced by the exponential decay (T_d) represented by

$$T_d = \frac{1}{kp^2} = \frac{4h^2}{k(2m-1)^2\pi^2} . \qquad (24)$$

This is a function of depth and friction, but for typical values ($k = .01\ m^2/sec$, $h = 50m$) it is on the order of 28 hours for the first term in the series to decay to 1/e of its initial value. This is the slowest term to decay.

The motion represented by (22) depends on the surface slope and thus new time scales are introduced into the solution. These depend on the horizontal dimensions represented and enter through the integration of the continuity equation (3). Time scales related to set up of the sea surface and seiche periods will govern the time rate of change of the surface slope. This change initiates the transients present in the geostrophic and bottom currents, which show the inertial rotation and exponential decay previously noted.

III. THE NUMERICAL SOLUTION

A. FORMULATION OF THE MODEL

1. Establishment of a Representative Cross Section

In formulating the numerical scheme it was decided to simplify the model by neglecting the derivatives along the y-axis. To accomplish this without the loss of any essential physics, it was decided to allow the seiche to oscillate across a narrow, shallow channel of infinite length. This prevents sea surface slopes from developing along the length of the channel but is otherwise non-restrictive. The simplification further reduces the problem to one of looking at a cross-sectional distribution of variables in the channel.

It was further decided to restrict the model by considering a cross-section of constant rectangular dimensions. The width and depth of the basin considered were fixed at 5000 meters and 30 meters respectively, and Figure 1 is a pictorial depiction of this cross section.

These simplifications allow eqs. (3) and (22) to be represented in the model as

$$\frac{\partial \xi}{\partial t} + \frac{\partial U}{\partial x} = 0 \qquad (25)$$

$$w(x,z,t) = \frac{2g}{h} \sum_{m=1}^{\infty} \frac{(-1)^m \cos(pz)}{p} \int_0^t e^{-(kp^2+if)(t-t')} \frac{\partial \xi}{\partial x}(t')\,dt' \qquad (26)$$

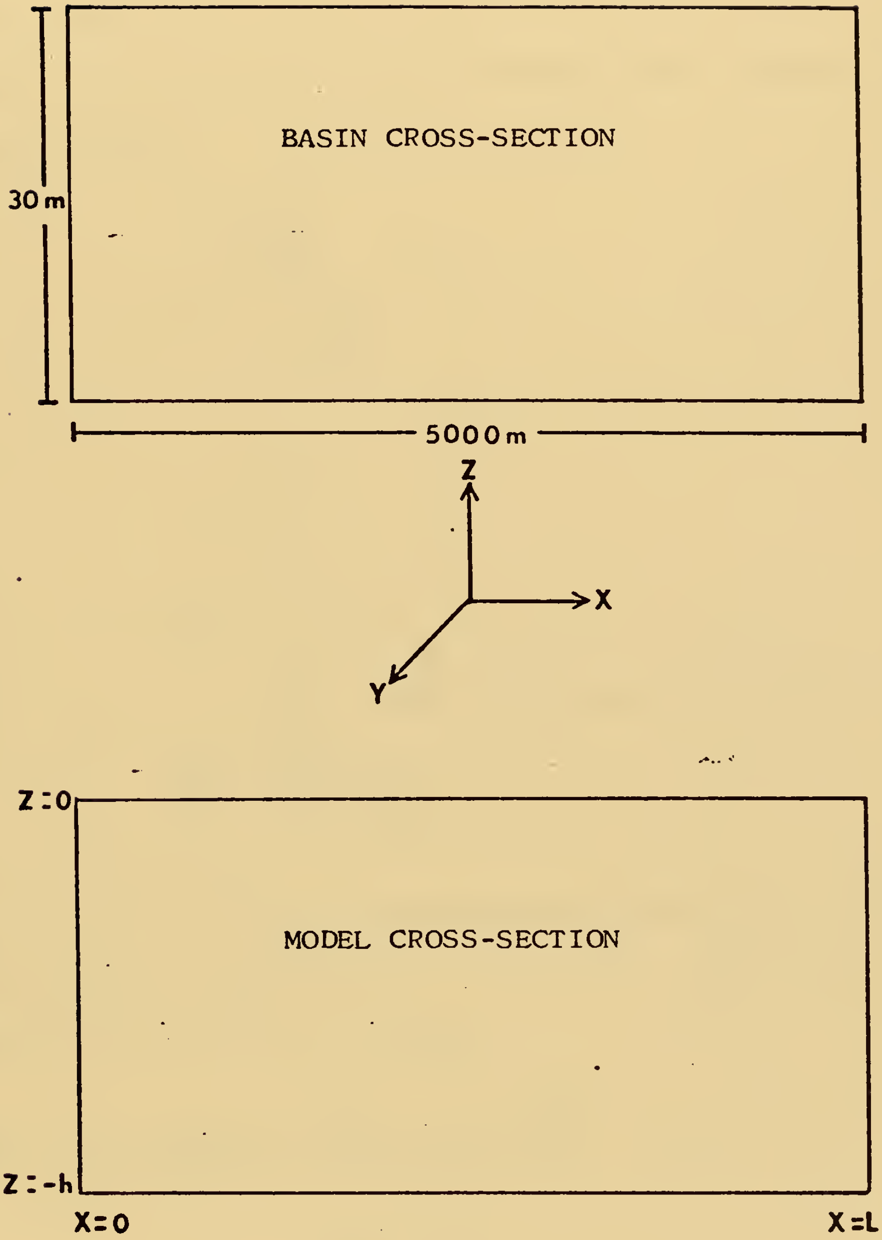

Figure 1. Pictorial Depiction of Model Basin

2. Establishment of Governing Non-dimensional Ratios

To represent the various time scales and frictional coefficients possible with more general time dependent motion the model was scaled to the period (T) of a free oscillating seiche in the model basin, and the coefficient of vertical friction determined by Ekman's "depth of frictional resistance (D)". Equation (26) was scaled as follows:

$$T = \frac{2L}{\sqrt{gh}} \quad ; \tag{27}$$

$$D = \pi \sqrt{\frac{2k}{f}} \; ; \tag{28}$$

Let,

$$t = Tt^*$$

$$t' = Tt'^*$$

$$dt' = T\, dt'^*$$

$$x = \frac{Lx^*}{10} \quad \text{(eleven grid points across the channel)}$$

$$\frac{\partial \xi}{\partial x} = \frac{10A_o}{L} \frac{\partial \xi^*}{\partial x^*}$$

where t^*, t'^*, ξ^*, x^*, are non-dimensional quantities and A_o is the free surface elevation at $x = 0$, $t = 0$. Substituting eqs. (27) through (29) into eq. (26) yields:

$$w = \frac{2g}{h} \sum_{m=1}^{\infty} \frac{(-1)^m \cos(pz)}{p} \frac{10A_o T}{L} \int_0^{t/T} e^{-(\frac{fD^2p^2}{2\pi^2} + if)(t-t')^* T} \times \frac{\partial \xi^*}{\partial x^*} dt'^* \; . \tag{30}$$

Recalling that $p = \frac{(2m-1)}{2} \frac{\pi}{h}$, and $\sigma = \frac{2\pi}{T}$, eq. (30) may be written

$$w = \frac{40g\,A_oT}{L} \sum_{m=1}^{\infty} \frac{(-1)^m \cos(pz)}{(2m-1)\pi} \int_0^{t/T} e^{-\{2\pi(\frac{f}{\sigma})\left[\frac{(2m-1)^2}{8}\,(\frac{D}{h})^2 + i\right](t-t')^*}$$

$$\times\ \frac{\partial \xi^*}{\partial x^*}\, dt'^* . \qquad (31)$$

It was determined that the two non dimensional ratios, (f/σ) and (D/h), appearing in eq. (30) govern the time/spacial scale and frictional dependence of the motion. For discussion and computation the first was designated (PCF) and the second (PCD).

The first of these ratios represents the relationship between the earth's inertial frequency and the frequency of the basin in the following manner.

$$f = 2\Omega \sin \phi$$

where Ω is the frequency of the earth's rotation and ϕ is the latitude.

$$\sigma = 2\pi F_m ,$$

where F_m is the resonance frequency of the basin. Since no external forcing terms were used in the solution, F_m is also the approximate frequency of the motion. Thus:

$$\frac{f}{\sigma} = \frac{\Omega \sin\phi}{F_m} .$$

The model was scaled for $(0 \le \text{PCF} \le 1)$. A value of (PCF = 0) represents motion of a time scale which occurs too quickly to be affected by Coriolis accelerations, while a value of (PCF = 1) represents motion whose time scale is equal to that of inertial rotation and subsequently greatly influenced.

The second term, PCD, is the ratio of the depth of frictional influence (Sverdrup, Johnson, and Fleming, 1942) to the actual water depth. The coefficient of vertical friction was determined in the model from eq. (28) as

$$k = \frac{(PCD \times h)^2 \times f}{2\pi^2} . \qquad (31a)$$

The model was scaled for $(0 \leq PCD \leq 2)$. A value of $(PCD = 0)$ represents a very deep basin where frictional effects on the motion are minimal, while $(PCD = 2)$ represents a basin where friction dominates the motion.

If the time scale of the motion being represented by the model is controlled strictly by the resonance of the basin, then the spacial scale of the basin is determined by a choice of PCD and PCF. PCD will govern the approximate depth of the basin while PCF determines the basin width through eq. (27). Certain conclusions about motion caused by external forces (i.e. tides, atmospheric pressure) producing time scales independent of the basin size were also inferred from the model and are discussed in the conclusions.

3. Adaptation of the Formal Solution to the Model

To establish two equations that could be solved simultaneously for sea surface elevation and transport, eq. (26) was integrated in the vertical using eqs. (4) and (8). Thus:

$$W(x,t) = \frac{-2g}{h} \sum_{m=1}^{\infty} \frac{1}{p^2} \int_0^t e^{-(kp^2+if)(t-t')} \frac{\partial \xi}{\partial x}(t')dt' \qquad (32)$$

and $W = U + iV$. Equation (32) represents the total volume transport associated with the flow at a particular point in the channel.

The real part of eq. (32) represents the cross-channel transport, while the imaginary part the along-channel transport.

The numerical scheme was established to solve eqs. (25) and (32) for ξ and W. The velocity profile, bottom stress, and energy balance associated with the flow were also recoverable from the scheme, and the details for this recovery will be discussed later.

4. Initial Conditions

The model assumes an initial state of rest in the motion and an initial set-up of the free surface. This was represented as

$$W(x,0) = 0, \tag{33}$$

and

$$\xi(x,0) = A_o \cos \frac{(\pi x)}{L}, \tag{34}$$

where $W = W(x,t)$ and $\xi = \xi(x,t)$.

5. Boundary Conditions

Since the governing equations were solved without reference to horizontal boundaries, these conditions had to be built into the model. The model therefore assumes no flow across the horizontal boundaries, or

$$W(0,t) = W(L,t) = 0. \tag{35}$$

These conditions were satisfied by requiring the surface slope to remain zero at these boundaries at all times. Therefore eq. (32) is forced to meet the conditions of eq. (35).

6. The Step-by-step Scheme

Both Welander and Galt suggested that a step-by-step numerical scheme could be used to solve eqs. (25) and (32). As a

first solution the staggered central difference scheme suggested by Galt was used and is summarized below.

$t = -\Delta t$ Given initial conditions on W.

$t = 0$ Given initial conditions on ξ.

$t = \Delta t$ Calculate W from eq. (32) using $\frac{\partial \xi}{\partial x}$ at $t = 0$.

$t = 2\Delta t$ Calculate ξ using an explicit finite-difference scheme on eq. (25) and U at $t = \Delta t$. Calculate a new surface slope.

$t = 3\Delta t$ . . . etc.

The term Δt is the time step of the explicit scheme.

This scheme was developed neglecting Coriolis $(f = 0)$ in eq. (32). The scheme proved to be stable and accurate subject to the following stability criterion:

$$\sqrt{gh}\,\frac{\Delta t}{\Delta x} < 1 \; . \tag{36}$$

The expression Δx is the spacial step across the channel. It was felt however that a more precise solution, not subject to such a restricted stability criterion, could be formulated using a totally implicit finite-difference scheme. The development of this method is now presented.

7. The Implicit Finite-difference Scheme

The implicit scheme used is a modification of a method described by Richtmyer and Morton (1967).

Start by approximating the time rate of change of the transport as follows:

$$\frac{\partial W}{\partial t} = \frac{(W)_{t+\Delta t} - (W)_t}{\Delta t} \tag{37}$$

From eq. (32)

$$\frac{\partial W}{\partial t} = \frac{1}{\Delta t}\left\{\frac{-2g}{h}\sum_{m=1}^{\infty}\frac{1}{p^2}\left[\int_0^{t+\Delta t} e^{-(kp^2+if)(t+\Delta t-t')}\,\frac{\partial\xi}{\partial x}(t')dt' - \int_0^{t} e^{-(kp^2+if)(t-t')}\,\frac{\partial\xi}{\partial x}(t')dt'\right]\right\} . \qquad (38)$$

By expanding the first integral as $\int_0^t + \int_t^{t+\Delta t}$ and regrouping terms, eq. (38) may be written as

$$\frac{\partial W}{\partial t} = \frac{1}{\Delta t}\left\{\frac{-2g}{h}\sum_{m=1}^{\infty}\frac{1}{p^2}\int_0^{t} e^{-(kp^2+if)(t-t')}\left(e^{-(kp^2+if)\Delta t}-1\right)\frac{\partial\xi}{\partial x}(t')dt'\right\}$$

$$+\frac{1}{\Delta t}\left\{\frac{-2g}{h}\sum_{m=1}^{\infty}\frac{1}{p^2}\int_t^{t+\Delta t} e^{-(kp^2+if)(t+\Delta t-t')}\,\frac{\partial\xi}{\partial x}(t')dt'\right\} \qquad (39)$$

Eqs. (25) and (32) can then be represented in the following form:

$$\left(\frac{\partial\xi}{\partial t}\right)_{t+\frac{\Delta t}{2}} = -\frac{1}{2}\left[\left(\frac{\partial U}{\partial x}\right)_t + \left(\frac{\partial U}{\partial x}\right)_{t+\Delta t}\right] \qquad (40)$$

$$\left(\frac{\partial W}{\partial t}\right)_{t+\frac{\Delta t}{2}} = \left(\frac{C1^*}{\Delta t}\right) + \left(\frac{C2^*}{2\Delta t}\right)\left[\left(\frac{\partial\xi}{\partial x}\right)_t + \left(\frac{\partial\xi}{\partial x}\right)_{t+\Delta t}\right] \qquad (41)$$

where

$$C1^* = \frac{-2g}{h}\sum_{m=1}^{\infty}\frac{1}{p^2}\int_0^{t} e^{-(kp^2+if)(t-t')}\left(e^{-(kp^2+if)\Delta t}-1\right)\frac{\partial\xi}{\partial x}(t')dt' \qquad (42)$$

$$C2^* = \frac{-2g}{h}\sum_{m=1}^{\infty}\frac{1}{p^2}\int_t^{t+\Delta t} e^{-(kp^2+if)(t+\Delta t-t')}dt' .$$

Equations (40) and (41) can be represented in Matrix form as follows:

$$\left(\frac{\partial\theta}{\partial t}\right)_{t+\frac{\Delta t}{2}} = A + \frac{B}{2}\frac{\partial}{\partial x}\left[(\theta)_t + (\theta)_{t+\Delta t}\right] \tag{43}$$

where,

$$\theta = \begin{Bmatrix} U \\ V \\ \xi \end{Bmatrix}$$

$$A = \begin{Bmatrix} C1/\Delta t \\ D1/\Delta t \\ 0 \end{Bmatrix}$$

$$B = \begin{vmatrix} 0 & 0 & C2/\Delta t \\ 0 & 0 & D2/\Delta t \\ -1 & 0 & 0 \end{vmatrix}$$

and,

$$C1 = \text{Real}\,\{C1^*\}\ ; \quad C2 = \text{Real}\,\{C2^*\}$$

$$D1 = \text{Imag}\,\{C1^*\}\ ; \quad D2 = \text{Imag}\,\{C2^*\}$$

(Real { } and Imag { } represent the real and imaginary part of the argument in braces).

The following implicit finite-difference equation was used to represent eq. (43):

$$\frac{\theta_j^{n+1} - \theta_j^n}{\Delta t} = A + \frac{B}{4\Delta x}\left[\theta_{j+1}^{n+1} - \theta_{j-1}^{n+1} + \theta_{j+1}^{n} - \theta_{j-1}^{n}\right] \tag{44}$$

where $\theta_j^n = \theta_{j\Delta x}^{n\Delta t}$

and n = (1,2,3,..., maximum number of time steps)

j = (1,2,3,..., J)

are the grid points in the time and x-directions respectively.

Letting

$$\alpha = \frac{\Delta t B}{4\Delta x}, \text{ and}$$

$$D_j = \alpha\theta^n_{j+1} + \theta^n_j - \alpha\theta^n_{j-1} + \Delta t A,$$

eq. (44) becomes

$$-\alpha\theta^{n+1}_{j+1} + \theta^{n+1}_j + \alpha\theta^{n+1}_{j-1} = D_j \ . \tag{45}$$

The left hand side of eq. (45) contains the unknown values of (θ) to be calculated, whereas the right hand side (D_j) are all known values.

A recursion relation of the following form was assumed.

$$\theta^{n+1}_j = E_j \theta^{n+1}_{j+1} + F_j \tag{46}$$

where

$$E_j = \begin{vmatrix} e^j_{11} & e^j_{12} & e^j_{13} \\ e^j_{21} & e^j_{22} & e^j_{23} \\ e^j_{31} & e^j_{32} & e^j_{33} \end{vmatrix}$$

and

$$F_j = \begin{Bmatrix} f^j_1 \\ f^j_2 \\ f^j_3 \end{Bmatrix}$$

If eq. (46) holds for all θ_j, then the model's left hand boundary conditions require that

$$E_o = \begin{bmatrix} 0 & 0 & 0 \\ 0 & 0 & 0 \\ 0 & 0 & 1 \end{bmatrix} \quad \text{and} \quad F_o = \begin{Bmatrix} 0 \\ 0 \\ 0 \end{Bmatrix} \tag{47}$$

Substituting the expression for θ_{j-1}^{n+1} derived from eq. (46) into eq. (45) yields:

$$\theta_j^{n+1} = \left[\frac{\alpha}{I+\alpha\ E_{j-1}}\right] \theta_{j+1}^{n+1} + \left[\frac{D_j-\alpha\ F_{j-1}}{I+\alpha\ E_{j-1}}\right] \tag{48}$$

Equating the right hand side of eq. (48) to eq. (46) gives the following recursion relationship:

$$E_j = \left[\frac{\alpha}{I+\alpha\ E_{j-1}}\right], \quad j \geq 1; \tag{49}$$

$$F_j = \left[\frac{D_j-\alpha\ F_{j-1}}{I+\alpha\ E_{j-1}}\right], \quad j \geq 1; \tag{50}$$

and I is the (3X3) identity matrix.

Using eqs. (47), (49), and (50), values of E_j and F_j were calculated inductively in order of increasing $j(j = 1,2,3,\ldots, J-1)$. Since the value of θ_{j+1}^{n+1} is given for $j = J-1$ by the model's right hand boundary condition ($U_J^n = V_J^n = 0$ and $\xi_{J-1}^n = \xi_J^n$), values of θ_j^{n+1} were then calculated inductively from eq. (46) in order of decreasing $j(j = J-1,\ J-2,\ \ldots\ ,\ 1)$. This completes the calculation of θ_j^{n+1} ($j = 1,2,3,\ \ldots\ ,\ J-1$). The details of the mathematics for representing E_j, F_j, D_j, and eq. (46) are presented in appendix A.

8. Numerical Treatment of $C1^*$ and $C2^*$

The numerical scheme for representing $C1^*$ and $C2^*$ is extremely lengthy and is merely outlined in this section. For a more detailed presentation the reader is referred to appendix B.

The integration of $C1^*$ was performed by dividing the total integration time into small time intervals (Δt) and assuming that the surface slope and effects of inertial rotation could be represented adequately by a constant throughout the interval. These values were calculated at the mid-point of each Δt interval and used in the scheme as representative values throughout the entire sub-interval. This permitted the integral to be evaluated analytically over each interval with a maximum error on the order of these approximations. Using these assumptions $C1^*$ was numerically represented as

$$C1^{*I}_{L} = \frac{-2g}{h} \sum_{M=1}^{MAXM} \left\{ \frac{1}{p^2} \left[\frac{1}{kp^2} (1 - e^{-kp^2 \Delta t}) \right] \sum_{N=1}^{I-1} \left[\left(\frac{\partial \xi}{\partial x}\right)^{N-\frac{1}{2}}_{L} (e^{-kp^2 \Delta t} e^{-if\Delta t} - 1) \right.\right.$$

$$\left.\left. X \, (e^{-if(I-\frac{1}{2}-N)\Delta t})(e^{-kp^2 (I-1-N)\Delta t}) \right] \right\} \qquad (51)$$

for $I = 2, 3, \ldots$, and $C1^{*1}_{L} = 0$. The value of the integer I ranges from 1 to MAXT (maximum problem time) and $I\Delta t$ represents the elapsed time from initial conditions. L takes on integer values from 1 to MAXL (maximum number of cross-channel grid points) and $L\Delta x$ is the distance from the left boundary. The integer M ranges from 1 to MAXM, and determines the maximum number of modes in the series that are included in the approximation of $C1^*$. It was determined from eq. (23) that MAXM = 25 would represent the solution with a maximum error of three percent, and this value was used throughout all

numerical evaluations. The integer N takes on the values from 1 to (I-1) and determines, through the exponential terms, how much rotation and decay has taken place in the recent time history of each transient considered. Since the terms of the series decay more rapidly with increasing friction (especially the higher modes), it was not necessary to carry their integration as far back as N = 1. It was decided to include only the terms of significant magnitude, and this was accomplished by requiring that when the value of $kp^2(I-1-N)\Delta t$ in eq. (51) was greater than 10, the corresponding terms were discarded.

The integration of $C2^*$ involves only one time interval (t to t+Δt). Again the amount of inertial rotation was evaluated at the mid-point and assumed constant throughout the interval, and $C2^*$ was evaluated as the following constant:

$$C2^* = \frac{-2g}{h} \sum_{M=1}^{MAXM} e^{-if(\frac{1}{2}\Delta t)} \left[\frac{1}{kp^2} (1-e^{-kp^2\Delta t}) \right] \quad (52)$$

$C1^*$ and $C2^*$ both contain the term

$\left[\frac{1}{kp^2} (1-e^{-kp^2\Delta t}) \right]$, and for k = 0 this term can not be numerically evaluated in this form. However this difficulty was overcome by expanding $e^{-kp^2\Delta t}$ in a Taylor series, i.e.

$$\left(1 - kp^2\Delta t + \frac{(kp^2\Delta t)^2}{2} - \frac{(kp^2\Delta t)^3}{6}\right) \quad (53)$$

and substituting this series for the term in eqs. (51) and (52) whenever the value of $kp^2\Delta t$ was less than 10^{-4}.

The method for separating the real and imaginary parts of $C1^*$ and $C2^*$ involves using the relation

$$e^{-ift} = \cos(ft) - i\sin(ft)$$

in eqs. (51) and (52) and gathering terms. The details are covered in appendix B.

9. Velocity Calculations

The velocity profiles across the channel were calculated by the model at discrete time intervals determined by an input parameter. Noting the simularity between the integral of eq. (26) and Cl^*, it was numerically possible to compute and store the terms of these integrals needed for velocity, during the calculation of Cl^*. For velocity profile computation, these stored values were recalled and applied in eq. (26). The details for numerically representing eq. (26) is also presented in appendix B.

10. Bottom Stress Calculations

The bottom stress (τ) associated with the motion was calculated using the following relation:

$$\tau = k\left(\frac{\partial w}{\partial z}\right)_{z=-h}$$

or from eq. (26),

$$\tau = \frac{2gk}{h}\sum_{m=1}^{\infty}\int_0^t e^{-(kp^2+if)(t-t')}\frac{\partial\xi}{\partial x}(t')dt' \ . \qquad (54)$$

Since the integral term of eq. (54) is identical to that of eq. (26), bottom stress is easily calculated whenever the velocity profile is recovered. Appendix B also contains the details for this calculation.

11. Energy Calculations

The total energy balance associated with the seiche is a sum of its potential and kinetic energy. This balance was

calculated as follows:

$$PE = \tfrac{1}{2} \rho \, g \int_0^L \xi^2 \, dx \qquad (55)$$

$$KE = \tfrac{1}{2} \rho \int_{-h}^{0} \int_0^L w^2 \, dx \, dz \qquad (56)$$

PE and KE are the potential and kinetic energies and (ρ) is the is the density of the water. Equations (55) and (56) were evaluated using Simpson's 1/3 rule (McCalla, 1967) whenever velocity was calculated.

The energy calculations were monitored during model testing as a calculational check since small numerical errors were quickly apparent in increasing energy levels.

12. Scaling of Model Output

Since the governing equations for the model were scaled to produce the ratios PCF and PCD, the output of the model must be appropriately re-scaled to obtain real values for the variables. The series of graphs were produced on a CALCOMP plotter with corresponding values from the model. The various axes were automatically scaled by the computer to fit the data being represented. These axes were then re-scaled using a non-dimensional scaling factor derived from the continuity equation to allow real values to be easily obtained. The exception is the figures depicting the energy balance, which are not scaled and should only be used to indicate relative changes in energy levels.

The scales for the various axes are as follows:

AXIS	SCALE
Surface Elevation	ξ/A_o
Time	$\frac{t\ (gh)^{\frac{1}{2}}}{2L}$
Velocity	$\frac{2w\ (h/g)^{\frac{1}{2}}}{C_1A_o}$
Transport	$\frac{2W}{C_2A_o(gh)^{\frac{1}{2}}}$
Bottom Stress	$\frac{2\tau(h)^{3/2}}{C_3A_okg^{\frac{1}{2}}}$

The values of g, h, k, A_o, L are determined from the actual basin being represented and C_1, C_2, C_3 are scaling constants dependent on the parameters of the prototype basin and the scaling of the graphs by the computer. These values are calculated for each figure and inserted in the scale. The variables, t, w, W, ξ, and τ are the real values associated with the basin being represented and may easily be obtained from the graphs by entering appropriate arguments for g, k, h, A_o, and L in the corresponding scale.

B. TESTING THE MODEL

1. Establishing a Reference Solution

One of the major difficulties in numerical analysis is verifying the accuracy and stability of the scheme. Since many numerical solutions deal with problems that have no analytical

solutions it is common practice to test the accuracy of these models against empirical data, or analytical solutions involving degenerate cases. As previously noted, data pertaining to time dependent flow is extremely scarce, and it was decided to test the accuracy of the model against a known analytical solution for the degenerate case where PCD = 0 (i.e. no friction). Analytical solutions to this case are readily available in the literature and a modification of one proposed by Prodman (1952) was used in the verification of the accuracy of the numerical scheme.

2. Accuracy and Stability of the Model

The accuracy of the model was determined by comparing the numerical representation of the free surface elevation at $(x = 0)$, the mid-channel transport, and the total energy balance, with the analytical values. Figures 2 through 5 highlite this comparison and indicate that the accuracy of the model was a function of time step (Δt) and the Coriolis parameter (f). It was noted that as the time step was reduced the numerical solution appeared to converge to the analytical solution. The phase shift in surface elevation over five periods was reduced from 45 degrees for $(\Delta t = T/20)$ to 24 degrees for $(\Delta t = T/40)$ and appeared to be independent of the value of Coriolis. This error might possibly be introduced into the system by approximating the sea surface slope as a constant value in the time history integration scheme. As (Δt) increases this linear approximation is extended over a greater time span and the resulting errors amplified. As the value of the Coriolis parameter was increased, the error in representing the amplitude of the free surface and total energy balance also increased, as

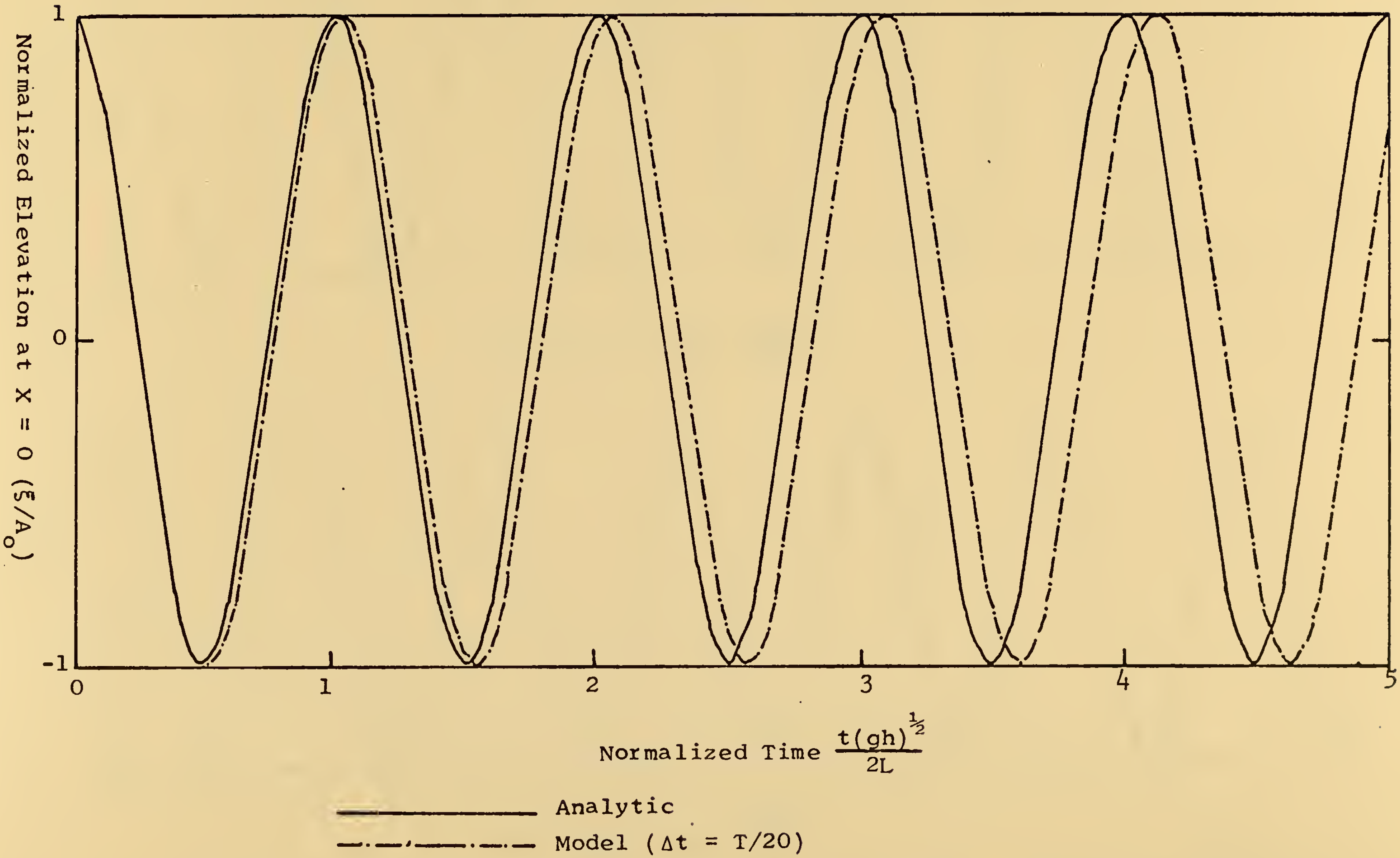

Figure 2. Comparison of Free Surface Elevation for Model and Analytic Solution (PCF = 0, PCD = 0).

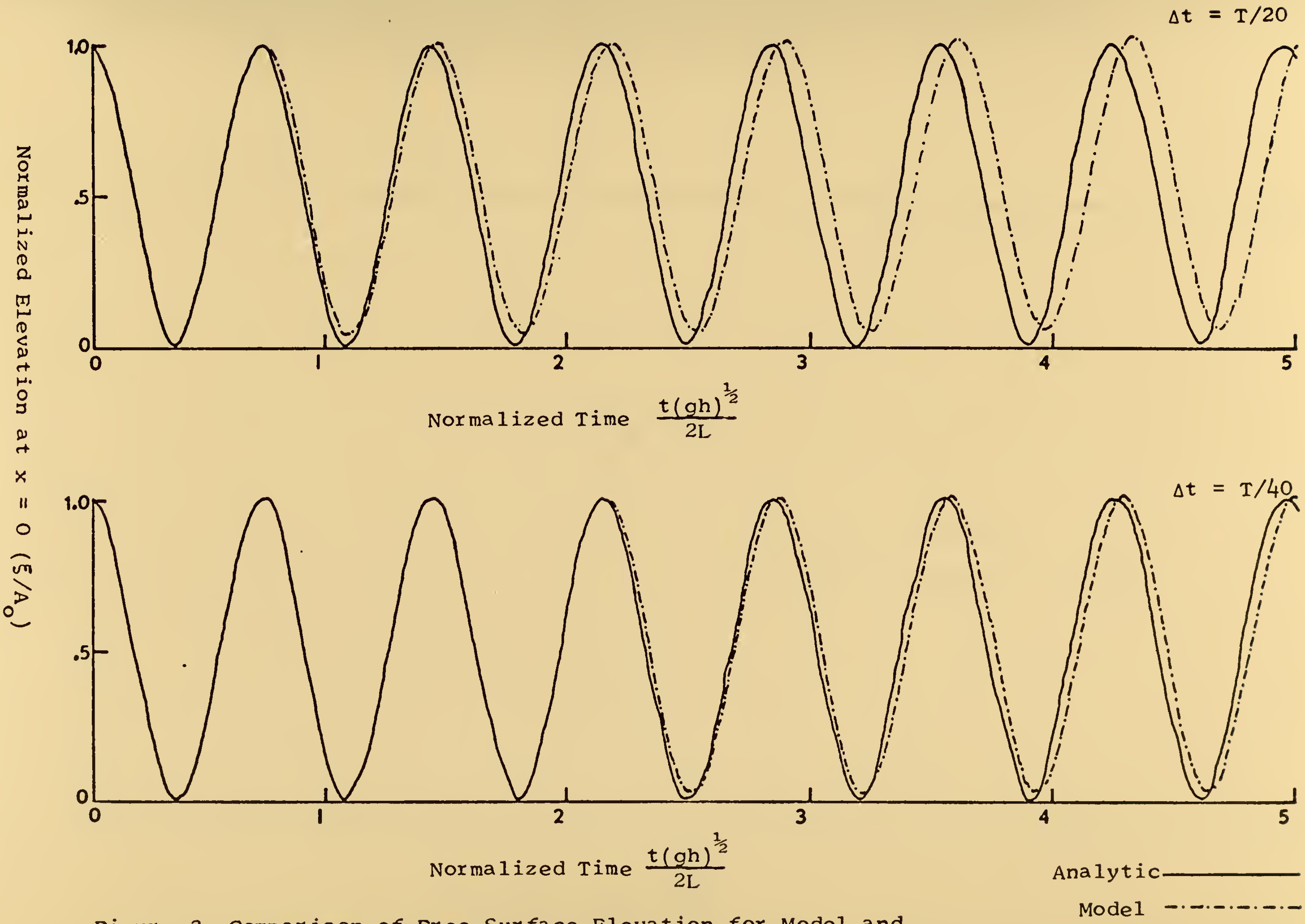

Figure 3. Comparison of Free Surface Elevation for Model and Analytic Solution (PCF = 1, PCD = 0).

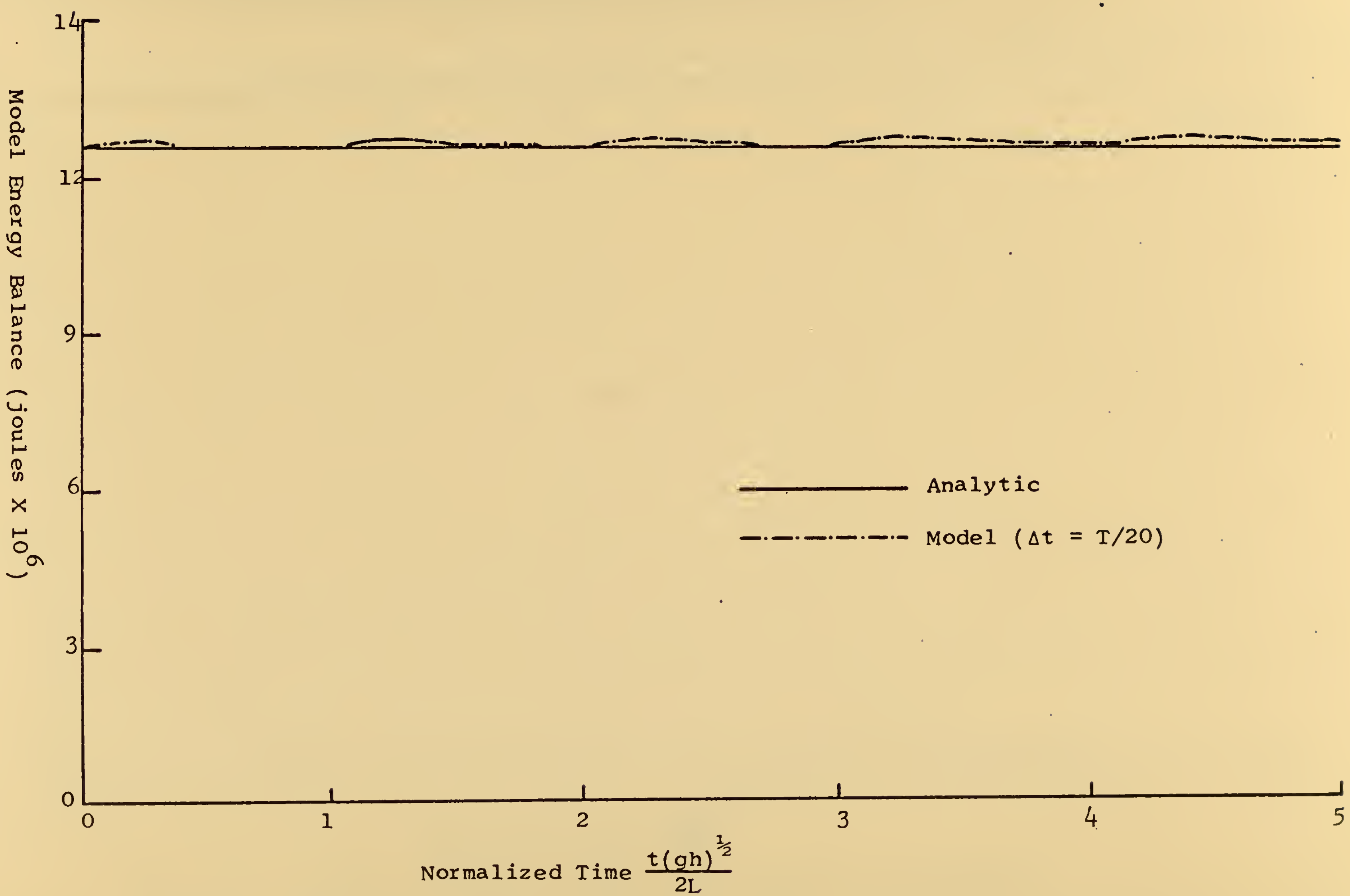

Figure 4. Comparison of Energy Balance for Model and Analytic Solution (PCF=0, PCD=0).

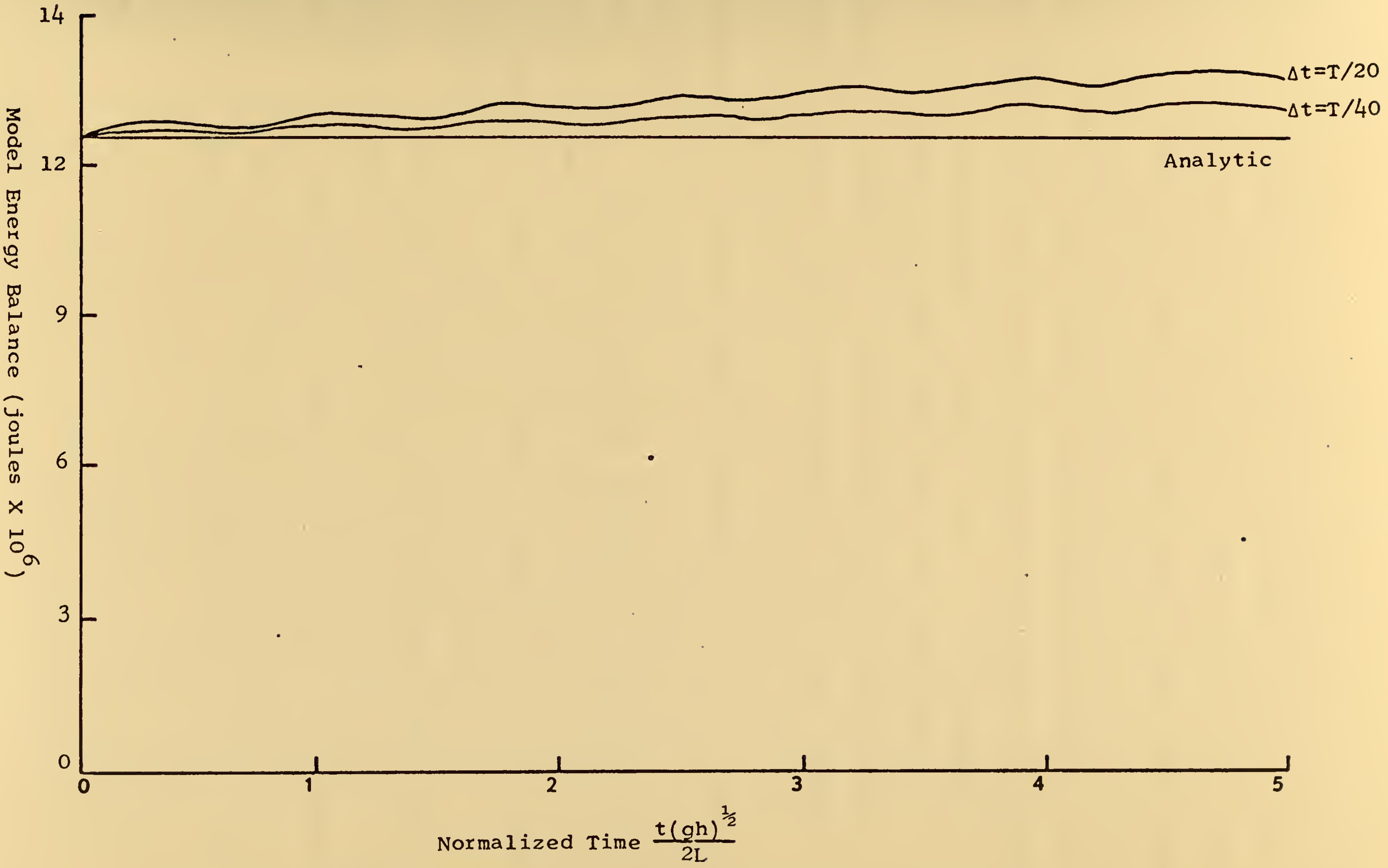

Figure 5. Changes in Energy Balance as a Function of Time Step.

depicted in Figures 3 and 5. The amplitude deviation was a maximum of one percentage for ($\Delta t = T/20$) and the energy rise was 8.5 and 3.7 percentage for ($\Delta t = T/20$) and $\Delta t = T/40$) respectively. Errors of this nature did not appear for solutions which neglected Coriolis, and possibly were introduced by approximating the amount of rotation [i.e. $e^{-if(t-t')}$] as a constant in the integration scheme. It is not exactly clear how this error increases the energy in the model but it was observed that it appeared linear and very systematic.

To determine whether this energy rise constituted a numerical instability, a standard Fourier series method (Smith, 1965) of stability analysis was attempted on eq. (44). However, due to the complicated nature of the amplification matrix, the eigenvalues could not be readily obtained and the analysis was abandoned. As an alternate test, the model was run with ($\Delta t = T/5$) for ($t = 5T$). This corresponds to $\left[\sqrt{gh}\,\frac{\Delta t}{\Delta x} > 3\right]$, and resulted in a further linear rise in the energy level. These errors were therefore judged to constitute a problem in numerical accuracy and not stability, for the range in which the test cases were run.

It was further found that the magnitudes of these errors could be predicted and controlled by varying the time step, and the model was run maintaining a maximum allowable error of one percent in the elevation and transport amplitude, and four percent rise in the total energy balance. This was accomplished by using a time step of ($\Delta t = T/20$) for ($PCF < .5$), and ($\Delta t = T/40$) for ($PCF \geq .5$). Since the errors in phase shift were strictly a function of time step, they were completely predictable and accounted for during data analysis.

It should be noted that for cases where friction is neglected (k = 0), the transients do not decay with time and must be carried throughout the integration scheme. Additionally, the bottom boundary condition degenerates to a free slip situation and the approximation of a constant velocity profile with a truncated cosine series becomes more inaccurate. The number of calculations increase rapidly as friction is decreased, which may introduce increasing errors in round-off.

Based on the comparison with the analytical solution it was concluded that the accuracy of the model could be sufficiently controlled such that the details of time dependent motion, as described by the governing integral and differential equations, could be adequately represented and examined.

C. MODEL LIMITATIONS

The most serious limitation imposed on the model were the basic assumptions of Ekman dynamics used in the formal solution of the governing equations. These assumptions were considered necessary to simplify the mathematical treatment of these equations to the extent that a numerical solution was feasible. The additioanl simplifications imposed during the formulation of the model further limit its capabilities. It was felt however that valuable experience in the techniques of numerically representing time dependent motion would be gained during the formulation of this simplified model, and insight gained from the numerical product. With this information available it might be possible to further refine the model and remove many of the more important restrictions. The

limitations inherent in the present model are listed in this section and the more important ones will be discussed in section (V) with recommendations for improving the scheme.

The basic assumptions made in arriving at eq. (22) have the following limiting effects of the model's capabilities: 1) the non-linear terms in the motion have been ignored; 2) a variation in the coefficient of vertical friction in the layer was not permitted; 3) the assumption of constant density neglects the effects of stratification on the pressure gradients in the layer, and the subsequent modification of the vertical momentum transfer; and 4) horizontal friction was considered insignificant and neglected.

Simplification of the model resulted in the additional limitation: 5) the assumption of a constant basin neglects the important effects of bottom topography on the flow. This is especially important for considering motion in shallow near shore areas where these effects are large.

IV. PRESENTATION OF RESULTS

A. TEST CASES AND GEOPHYSICAL SIMULATIONS

1. Description of Test Cases

In order to gain maximum insight into the physical processes occurring in the motion, as well as to study the effects of inertial rotation and friction on the variables, the model was run for 25 test cases in the ranges of $(0 \leq PCF \leq 1)$ and $(0 \leq PCD \leq 2)$. Table I summarized the various controlling parameters of each run and includes the Central Process Unit (CPU) time used on the IBM 360/67 system for each program.

2. Description of Geophysical Simulations

As interesting dynamic interactions developed in the test cases, it was decided to simulate actual geophysical embayments to determine to what extent these phenomena were present and significant. The actual length, depth, and latitude of the basins were measured and used to calculate (f), (σ), and (PCF). An Ekman depth of 20 meters was assumed in the calculation of (PCD). Runs 26-30 represent these simulations and the various imput parameters are summarized in Table II.

B. DISCUSSION OF TEST RUN RESULTS

1. Frictional Effects on the Flow

To describe the conditions where friction totally dominates the motion, the model was run with varying amounts of friction and $(PCF = 0)$. It must be noted that by neglecting the effects of inertial rotation, the Ekman depth is no longer specified as

Table I. Parameters of Test Cases (runs 1-25)

RUN NO.	PCF	PCD	CPU(MIN-SEC)
1	.25	.5	6-2
2	.25	1.0	3-51
3	.25	1.5	3-8
4	.25	2.0	2-49
5	0	.5	5-11
6	0	1.0	3-20
7	0	1.5	2-43
8	0	2.0	2-24
9	0	0	13-33
10	.25	0	14-58
11	.5	2.0	6-25
12	.75	2.0	6-0
13	1.0	2.0	5-48
14	.5	1.5	7-25
15	.75	1.5	6-42
16	1.0	1.5	6-25
17	.5	1.0	9-40
18	.75	1.0	8-21
19	1.0	1.0	7-40
20	.5	.5	16-14
21	.75	.5	13-52
22	1.0	.5	12-29
23	.5	0	62-48
24	.75	0	62-38
25	1.0	0	62-51

NOTES: For the model basin

10 $T = 583.2$ Sec

2) $\sigma = .108 \times 10^{-1}$ Sec^{-1}

Table II. Parameters of Geophysical Simulation

BASIN	RUN	h(m)	L(m)	LAT.	$f(\text{Sec}^{-1})$	PCD	PCF	$\sigma(\text{Sec}^{-1})$	CPU(MIN-SEC)
Monterey Bay	26	72	15,000	$36^\circ 21'$	.862E-4	.28	.155E-1	.556E-2	15-53
South San Francisco Bay	27	10	9,600	$37^\circ 35'$	.887E-4	2.0	.261E-1	.340E-2	7-31
Chesapeake Bay	28	27	45,000	38°	.895E-4	.73	.783E-1	.114E-2	13-39
Lake Erie	29	22	90,000	42°	.973E-4	.91	.190	.512E-3	11-49
Long Island Sound	30	27	30,000	41°	.954E-4	.73	.556E-1	.172E-2	13-21

NOTE: $E\text{-}4 = 10^{-4}$

evidenced by eq. (28). Therefore, the frictional coefficients generated by runs 1 through 4 were artificially imposed on the model with (PCF = 0), and resulted in runs 5 through 8.

The results for these cases are depicted in Figures 6 through 8 and are simply a seiche damped by friction. As the friction coefficient increased the damping of the motion increased with a resulting increase in the period of oscillation. For the maximum case of (PCD = 2), the seiche was completely damped after 4½ periods. These results were completely predictable and are presented to show that the model's representation of motion which is dominated by friction conforms to previous observations. (Pierson and Neuman, 1966)

An interesting coupling between bottom stress and transport developed during these cases and a typical example is depicted in Figure 9. In all cases examined a phase lag quickly developed between the transport and the bottom stress. For the case showed, the value of this lag averaged 45 degrees through the periods of oscillation. This phase lag can be explained by recalling that the transport is an integration of the motion over the entire water column, whereas the bottom stress is solely dependent on the velocity gradient at the bottom. Since friction has its greatest effect at the bottom, changes in magnitude and direction of the flow nearly always initially occur next to this boundary and propagate upwards in the column. The result is that changes in transport always lag changes in the bottom velocity gradient and consequently the bottom stress. This phase lag has obvious effects on the accuracy of commonly used numerical schemes where bottom

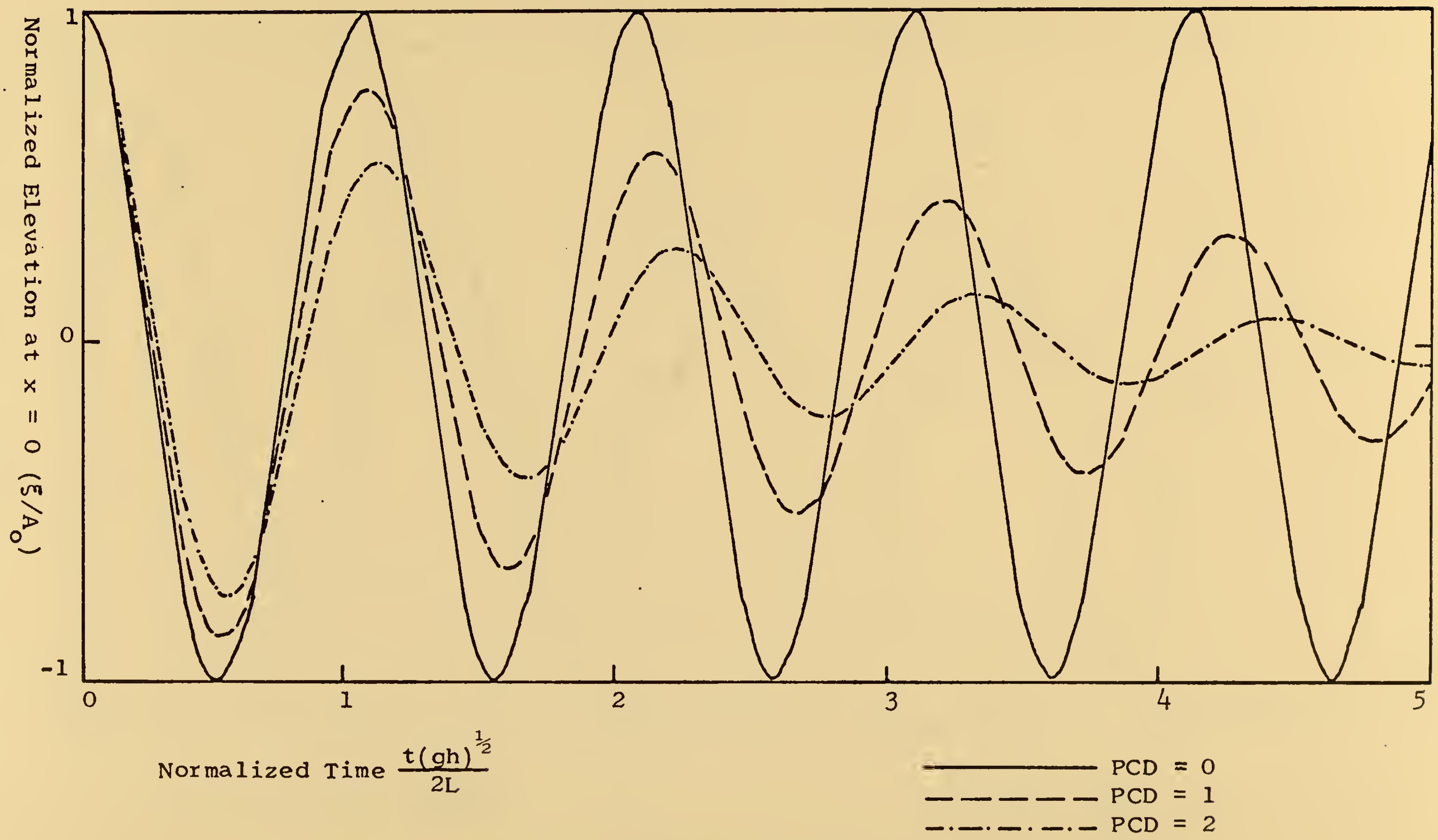

Figure 6. Effects of Friction on the Free Surface (PCF = 0).

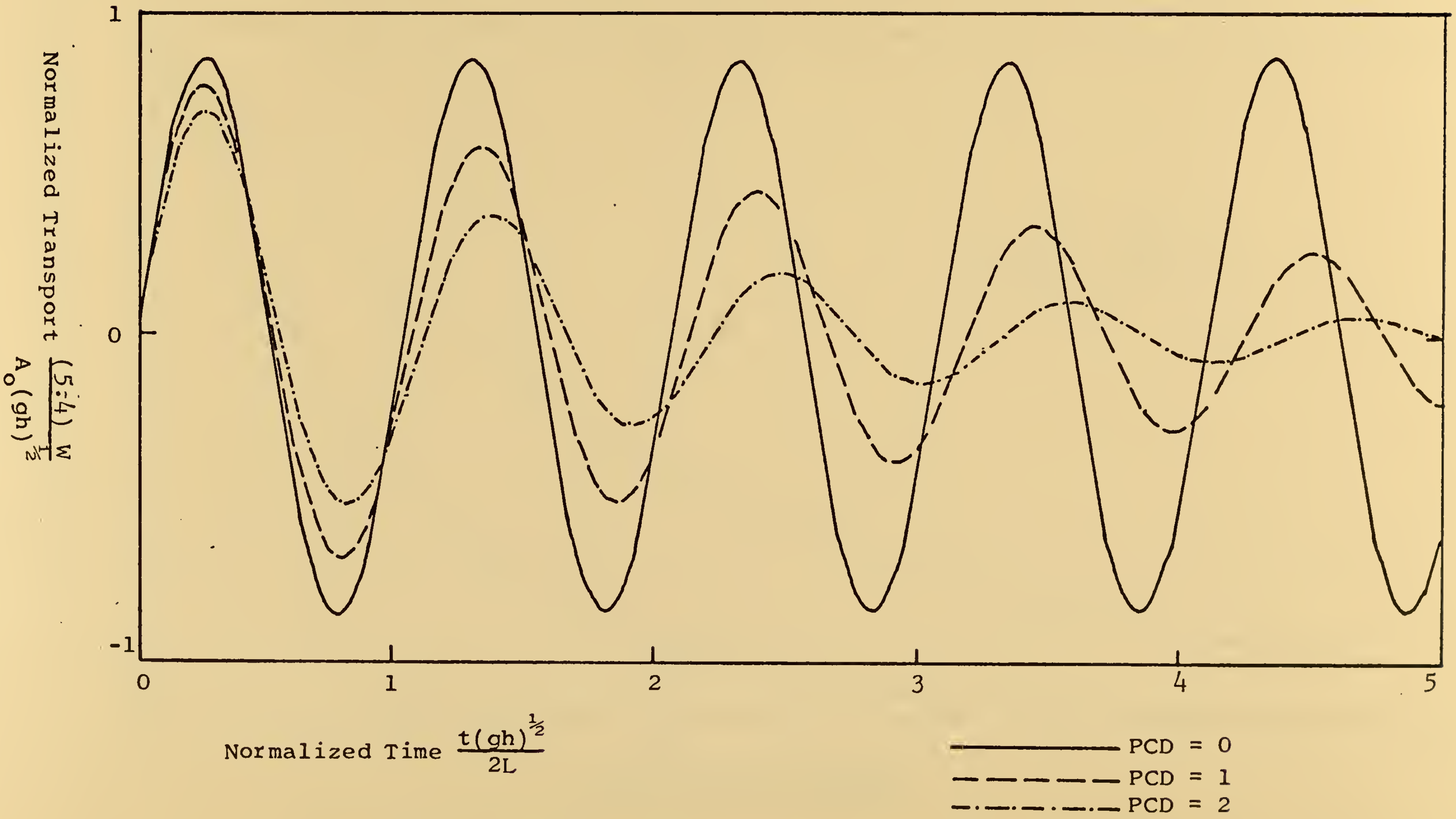

Figure 7. Effects of Friction on Mid-channel Transport (PCF = 0).

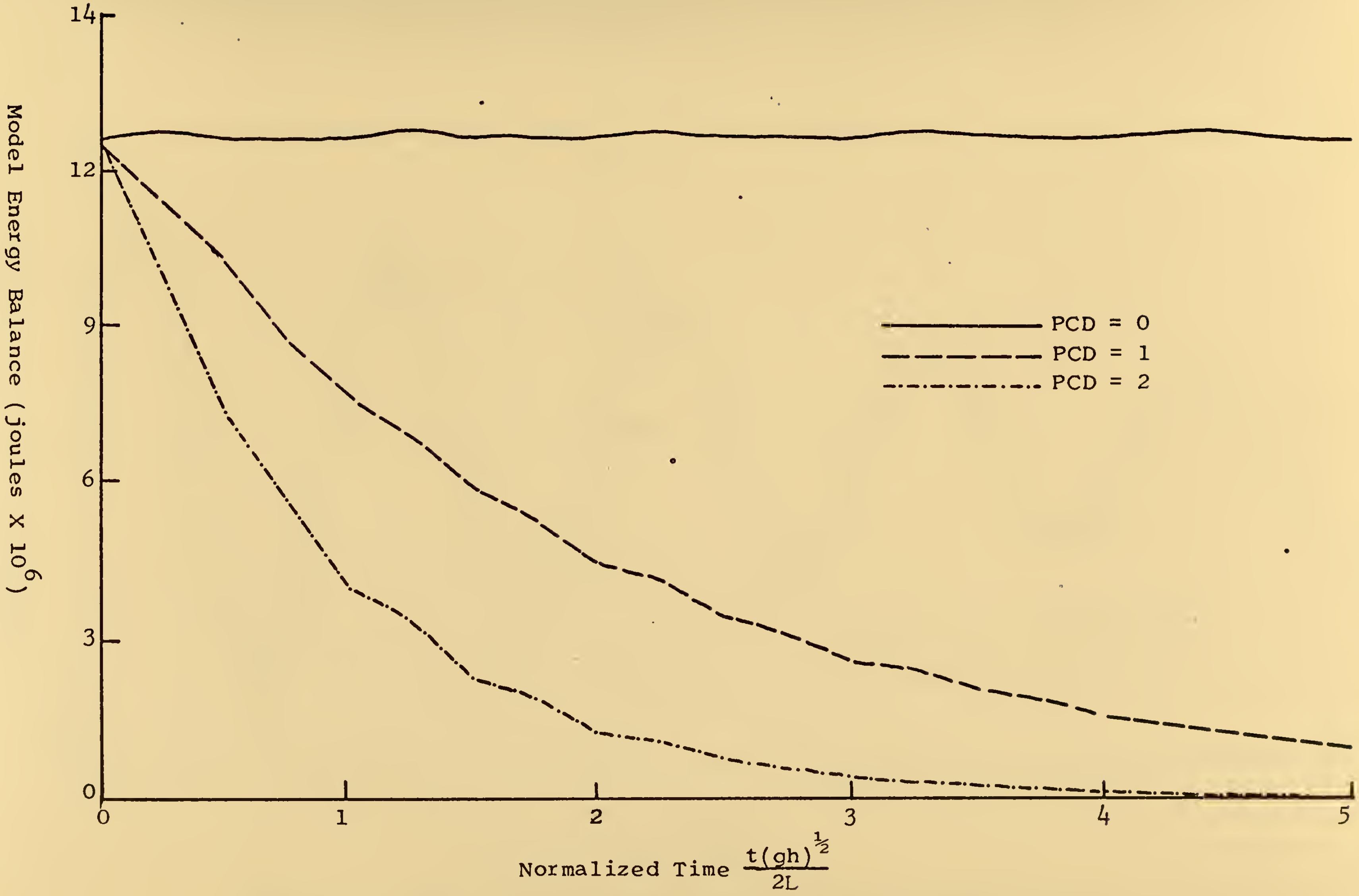

Figure 8. Effects of Friction on Energy Balance (PCF = 0).

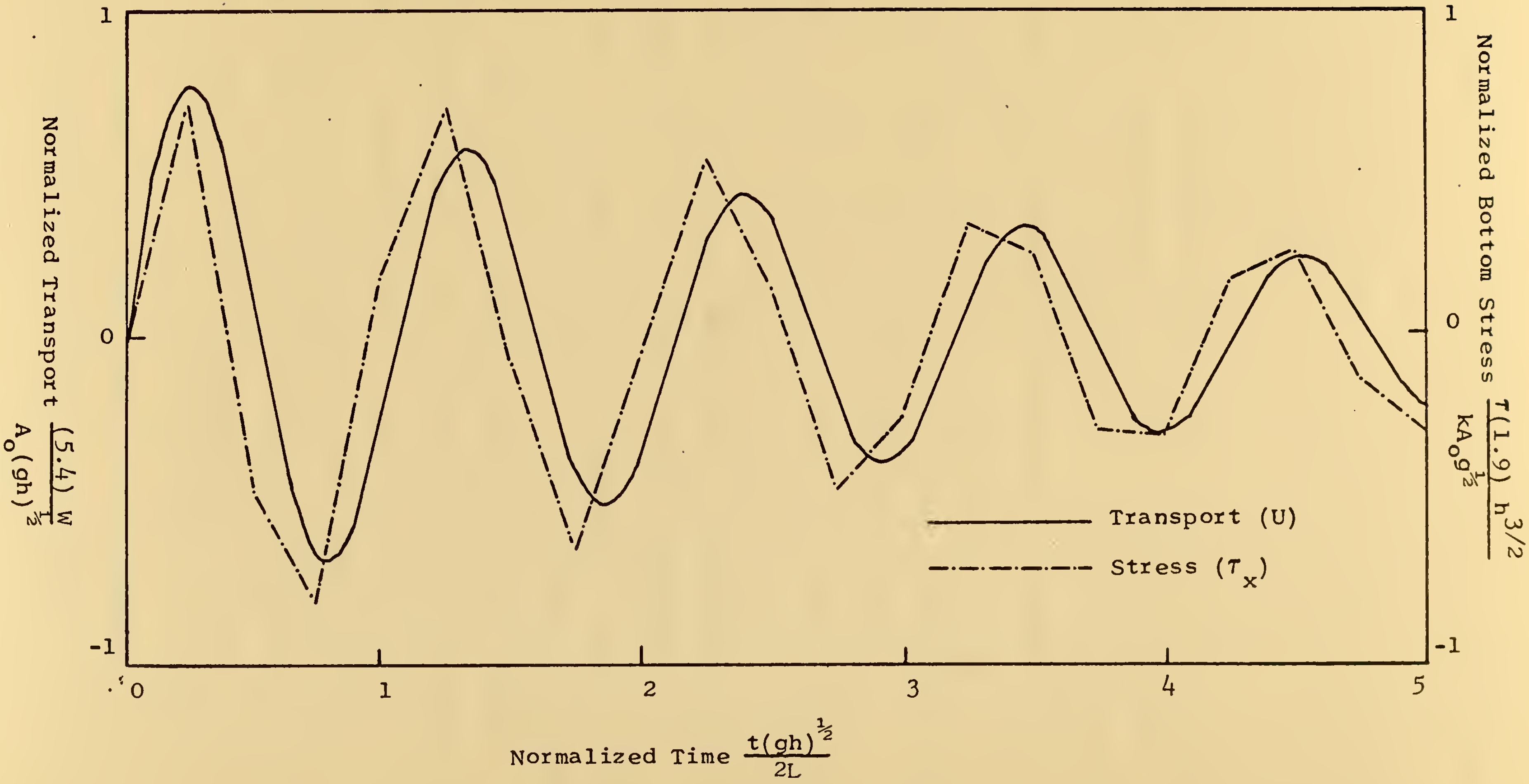

Figure 9. Comparison of Bottom Stress and Mid-channel Transport (PCF=0, PCD=1).

stress is parameterized in terms of the transport. This technique places strong restrictions on possible interactions between the flow and the bottom, and although it may be sufficient for approximating steady state problems, it is unlikely that it will represent transient motion very well.

Figure 10 represents typical velocity profiles for motion which is totally dominated by the effects of vertical friction. The increased period of oscillation and the mechanism causing the phase lag between the transport and the bottom stress is clearly evident. At times (t = T/2) and (t = 3T/4) the profiles are in transition from being totally positive to totally negative, and the transport and bottom stress are 180 degrees out of phase.

These velocity profiles are typical of those found in other boundary layer flow and are similar to the wind profiles observed at the air sea interface over smooth water. They indicate that the stability of the flow has a strong frictional dependence. At (t = T/4) and (t = T) the profiles are maximum and, except initially in the upper layers, friction exerts a strong influence throughout the column. The result is a smooth regular flow and a well developed frictional boundary layer with the region of greatest shear at the bottom. During the transition phases (t = T/2 to t = 3T/4) the profile changes direction and the water column appears to be less stable. The velocities in the column are minimum just prior to and after reversal and thus the influence of friction in the column is reduced. This region of reduced frictional influence moves up the column at the point where the flow changes direction. As the flow completes its reversal and the velocities in the column

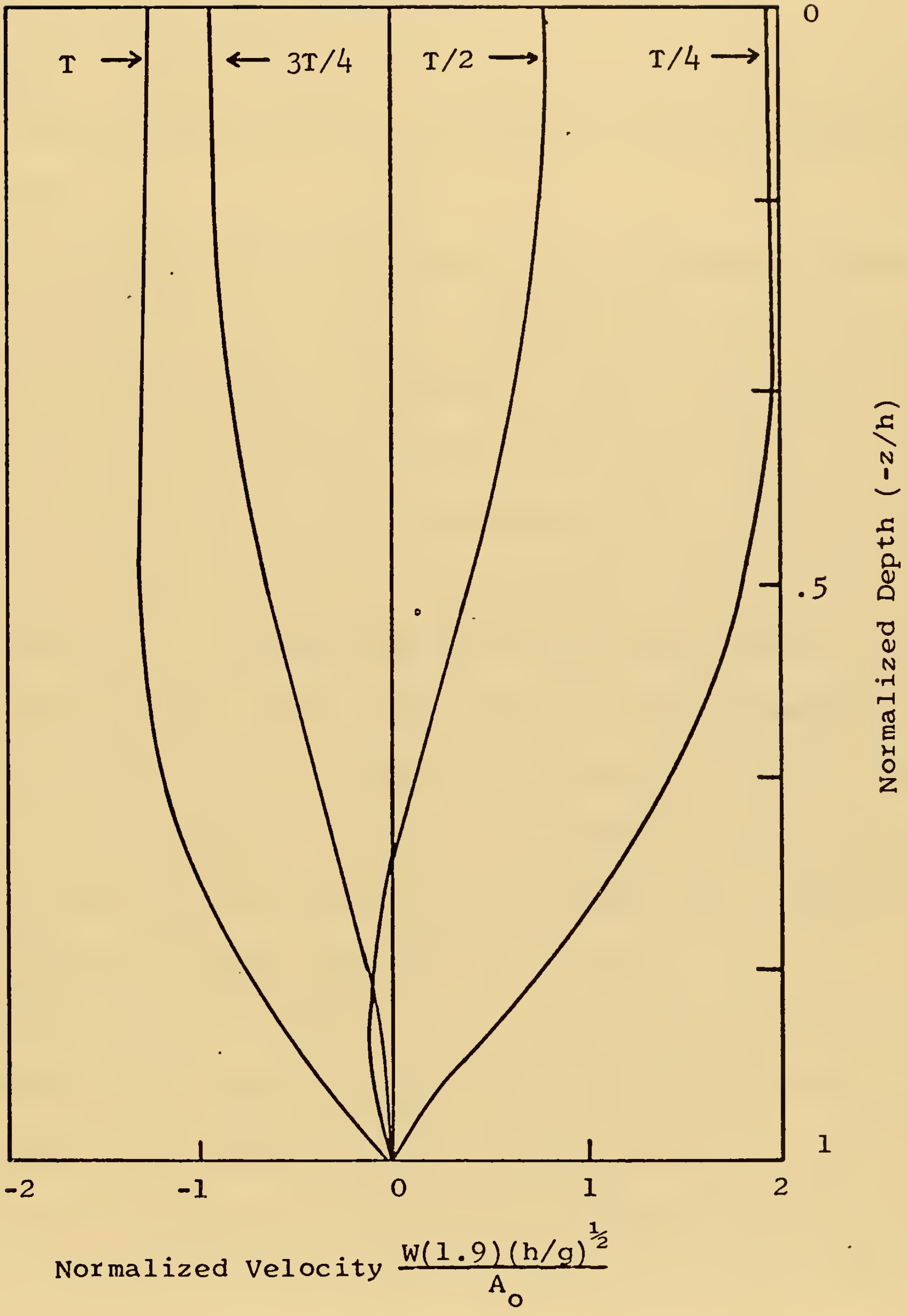

Figure 10. Effects of Friction on Mid-channel Velocity (PCF = 0, PCD = 2).

increase, the effect of strong frictional influences is quickly re-established throughout the layer, the region of maximum shear shifts to the bottom, and smooth flow once again prevails at time (t = T).

2. Coriolis Effects on the Flow

To gain insight into how inertial rotation modifies the transient motion, runs 10, and 23 through 25 were made neglecting friction (PCD = 0).

It is important to realize that the relationship between the transport and the free surface elevation for a non rotational, frictionless seiche, as seen in Figures 6 and 7, is similar to the velocity/elevation relationship of the frictionless pendulum. At (t = 0), (t = T/2), and (t = T), the energy of the seiche is entirely potential, whereas at (t = T/4) and (t = 3T/4) it is entirely kinetic. At intermediate times the energy balance is a combination of potential and kinetic and is totally conserved. The free surface elevation and transport periodically oscillate between maximum positive and negative values of respectively equal magnitudes, always maintaining their constant phase shift. Figure 2 represents this oscillation for the free surface.

As the effects of Coriolis acceleration were introduced into the model these conservative oscillations were greatly modified as can be seen from a comparison of Figures 2, 3, 11, and 12. The effect of a moving earth is that the total potential energy of the surface elevation will not be available for transfer to kinetic energy since the water particles are forced to turn due to the Coriolis Acceleration. Although the energy balance still remains

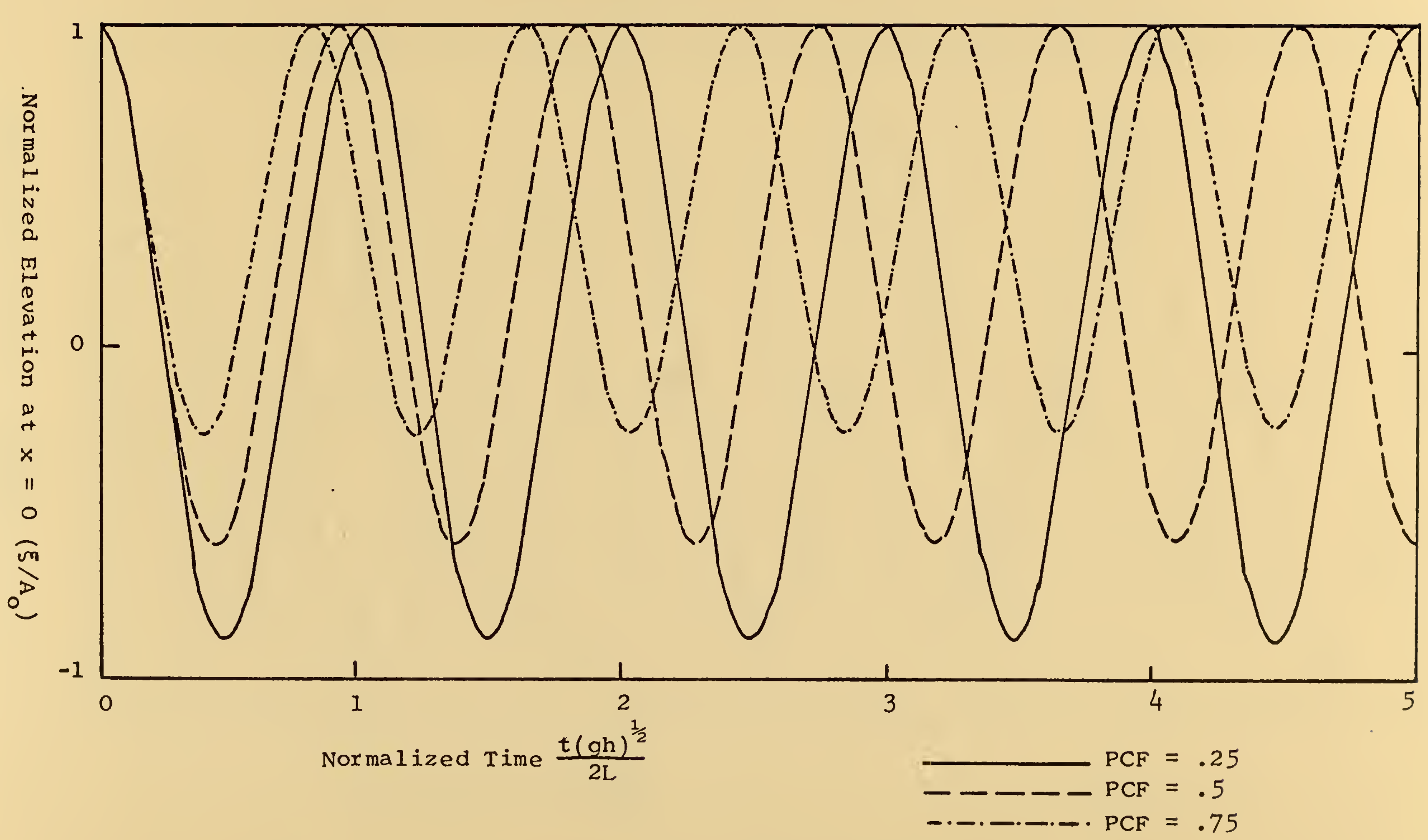

Figure 11. Effects of Inertial Rotation on Surface Elevation (PCD = 0).

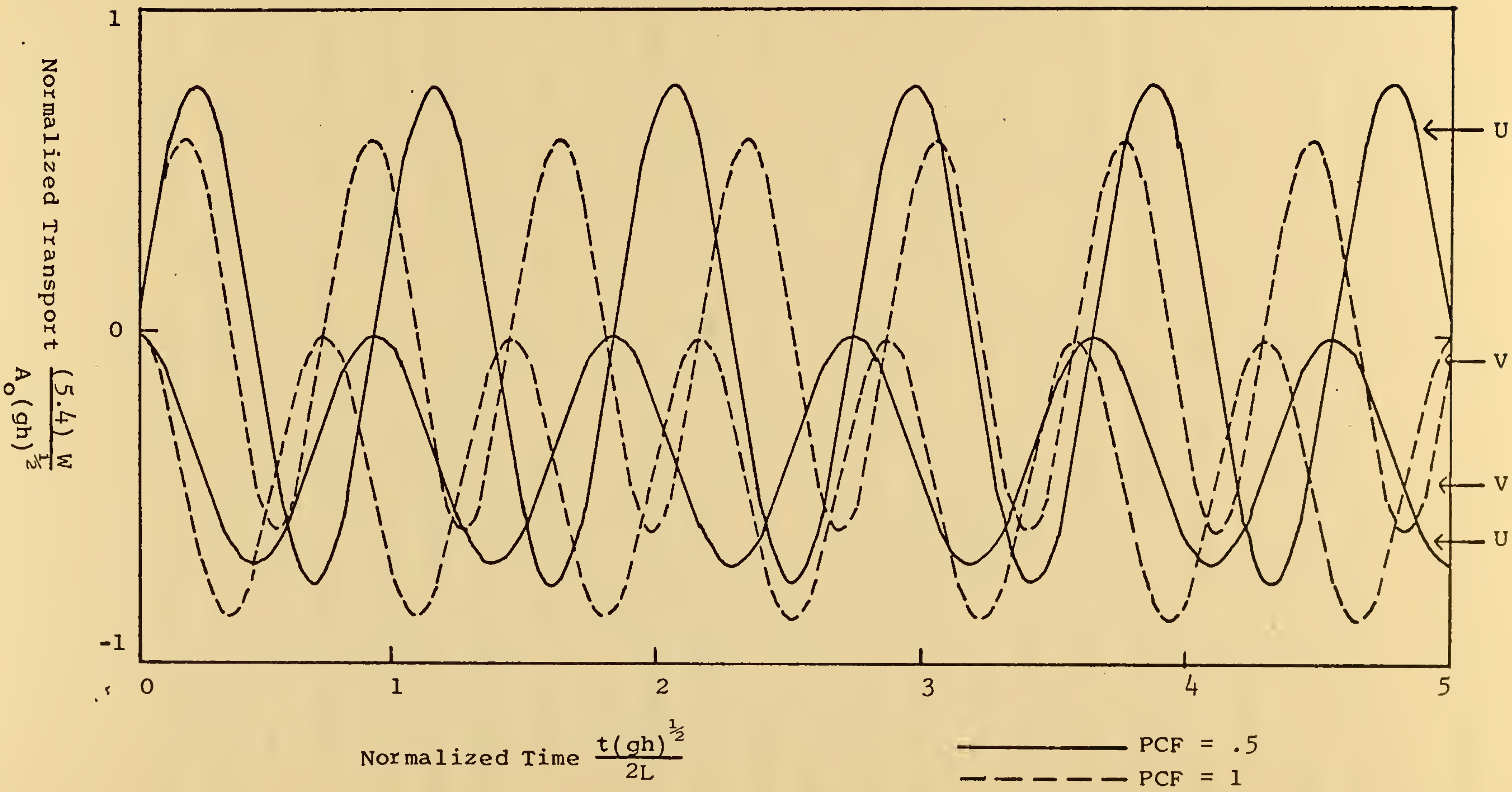

Figure 12. Effects of Inertial Rotation on Mid-channel Transport (PCD = 0).

conservative, the relationship between the free surface elevation and the flow changes significantly.

To understand how rotation acts to modify the flow, consider first the physical processes which drive the system. These are discussed in terms of the frictionless irrotational seiche. The initial conditions for the model were identical for all runs; that of a positive set-up of the free surface at the left boundary (x - 0) and no motion in the basin (a condition of static equilibrium). As the system is released the pressure gradients developed by this set-up start the fluid moving in the positive x-direction resulting in a net divergence in the left side of the channel and convergence in the right. The free surface responds to this flow by slumping at the left and rising at the right with equal magnitudes. At time (t = T/4) the surface is level (i.e. no gradients) and the kinetic energy associated with the flow is equal to the potential energy of the initial free surface set-up. Therefore the surface continues to fall at the left and rise at the right until this kinetic energy has been entirely converted into potential energy and a state of momentary equilibrium is once again reached. The sea surface is now set up at the right boundary equal in magnitude to the initial conditions, the pressure gradients equal but opposite to the initial values, and the flow reverses direction and the system returns to initial conditions, etc. It is important to realize that only the divergence of the flow in the cross-channel direction can influence the system because no gradients are allowed to develop along the length of the channel.

With these processes in mind the observed effects of rotation on the system can adequately be explained. With the initial set-up previously described, the flow will start in the same manner. As soon as the motion begins however, the Coriolis acceleration will start to turn the flow in the negative y-direction (left rotation), and a component of the flow will start to develop along the axis of the channel. Therefore some of the potential energy is converted into rotational kinetic energy. The amount of rotational kinetic energy that the system receives is a function of the velocity of the flow, the value of Coriolis, and the time scale of the motion. The slumping of the surface elevation at the left and rising at the right will continue as long as there is divergence in the positive x-direction; however since a certain amount of energy is rotational, the set-up at the right boundary can not achieve the magnitude of initial conditions. When the cross-channel flow vanishes the entire motion is in the along channel direction, with subsequent rotation turning the flow back in the direction from which it initially came. It should be noted that for a maximum value of (PCF = 1), Figure 3 shows the free surface elevation at the left boundary never falling below the horizontal.

An interesting relationship developed in the transport as rotation was introduced into the system, resulting in a rectification of the along channel component of the transport (V). An examination of Figure 12 showed that the cross-channel transport (U) periodically oscillates between maximum positive and negative values while the along channel component oscillated between zero and a maximum in one direction. It was easily demonstrated that this

direction is strictly a function of initial set-up. As the flow was initiated in the positive x-direction the initial along channel component developed in the negative y-direction. When the cross-channel flow reverses direction, along channel components are generated in the positive y-direction. These components are just sufficient to cancel the components previously established in the opposite direction, resulting in a rectification in the along-channel transport. For motions of large time scales, this process implies that important changes in the flow are caused by Coriolis accelerations and these will be discussed in the conclusions.

Another observed feature of rotation was the subsequent reduction in oscillation period for increased values of Coriolis. The effect of rotation in reducing the spacial scale of the motion allows the system to oscillate with greater frequency.

It is apparent from the previous discussions that the effects of inertial rotation can not be neglected when dealing with large time scale motion.

3. Combined Effects of Friction and Coriolis

The remainder of the test runs were used to investigate how friction and inertial rotation in various combinations effect the transient motion. Some of the important consequences are depicted in Figures 13 through 17.

The phase shift difference between bottom stress and transport existed throughout all values of (PCF) and (PCD), as evidenced in Figures 13 and 14. This phase lag occurred in varying degrees but was a definite characteristic of time dependent motion, vanishing only when the motion became critically damped.

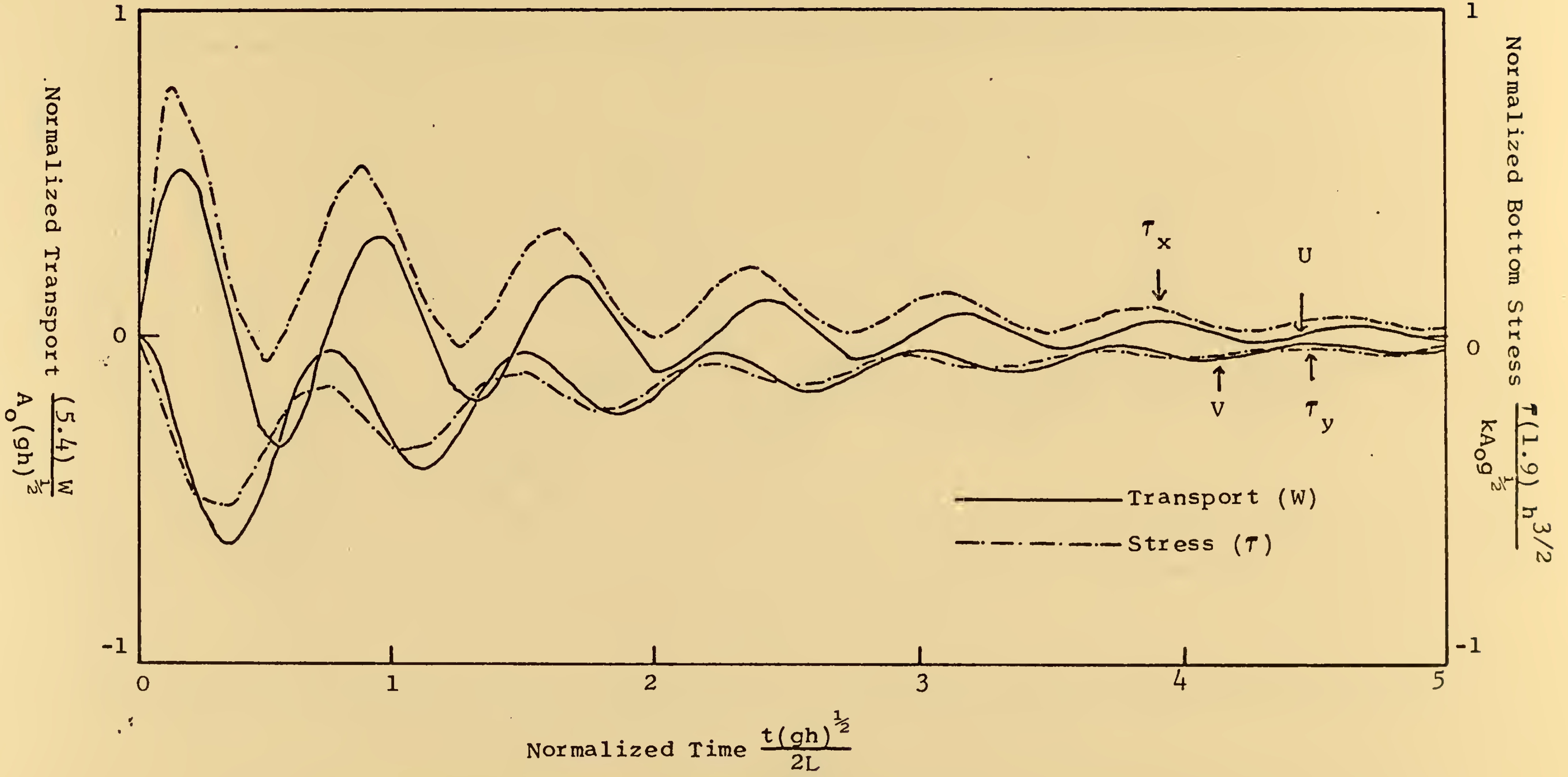

Figure 13. Comparison of Bottom Stress and Mid-channel Transport (PCF = .5, PCD = 1).

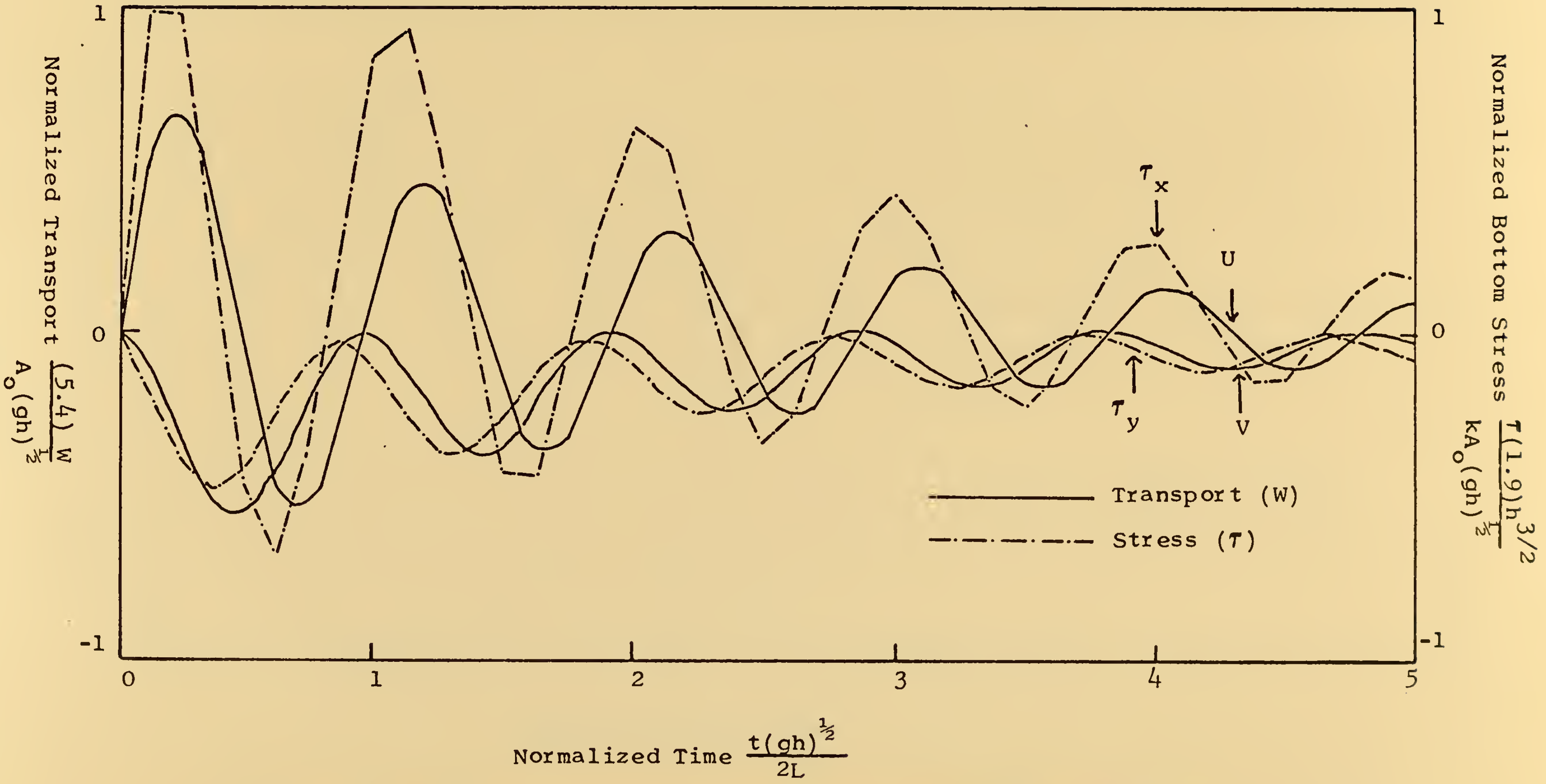

Figure 14. Comparison of Bottom Stress and Mid-channel Transport (PCF = 1, PCD = 1).

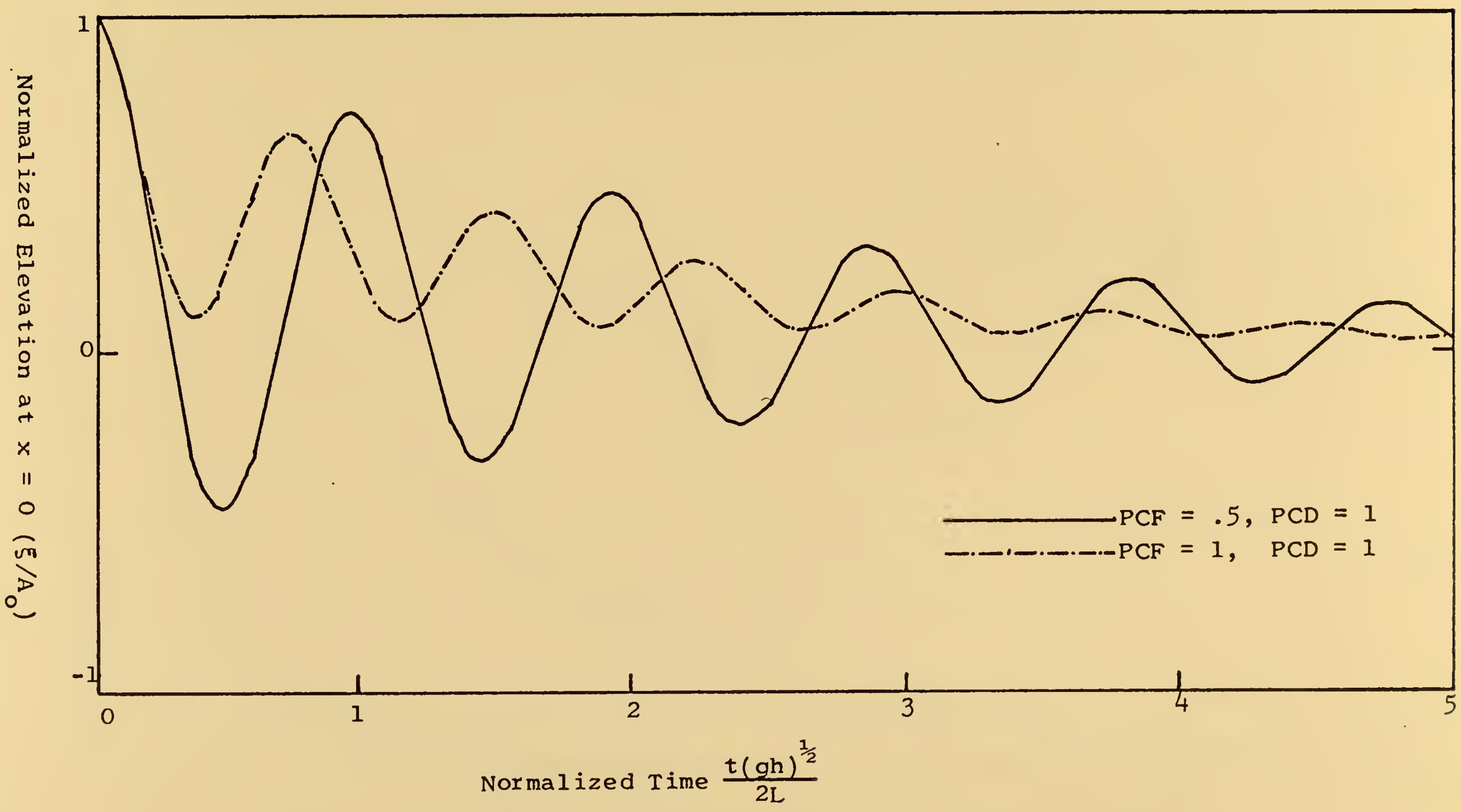

Figure 15. Effects of Friction and Coriolis on the Free Surface.

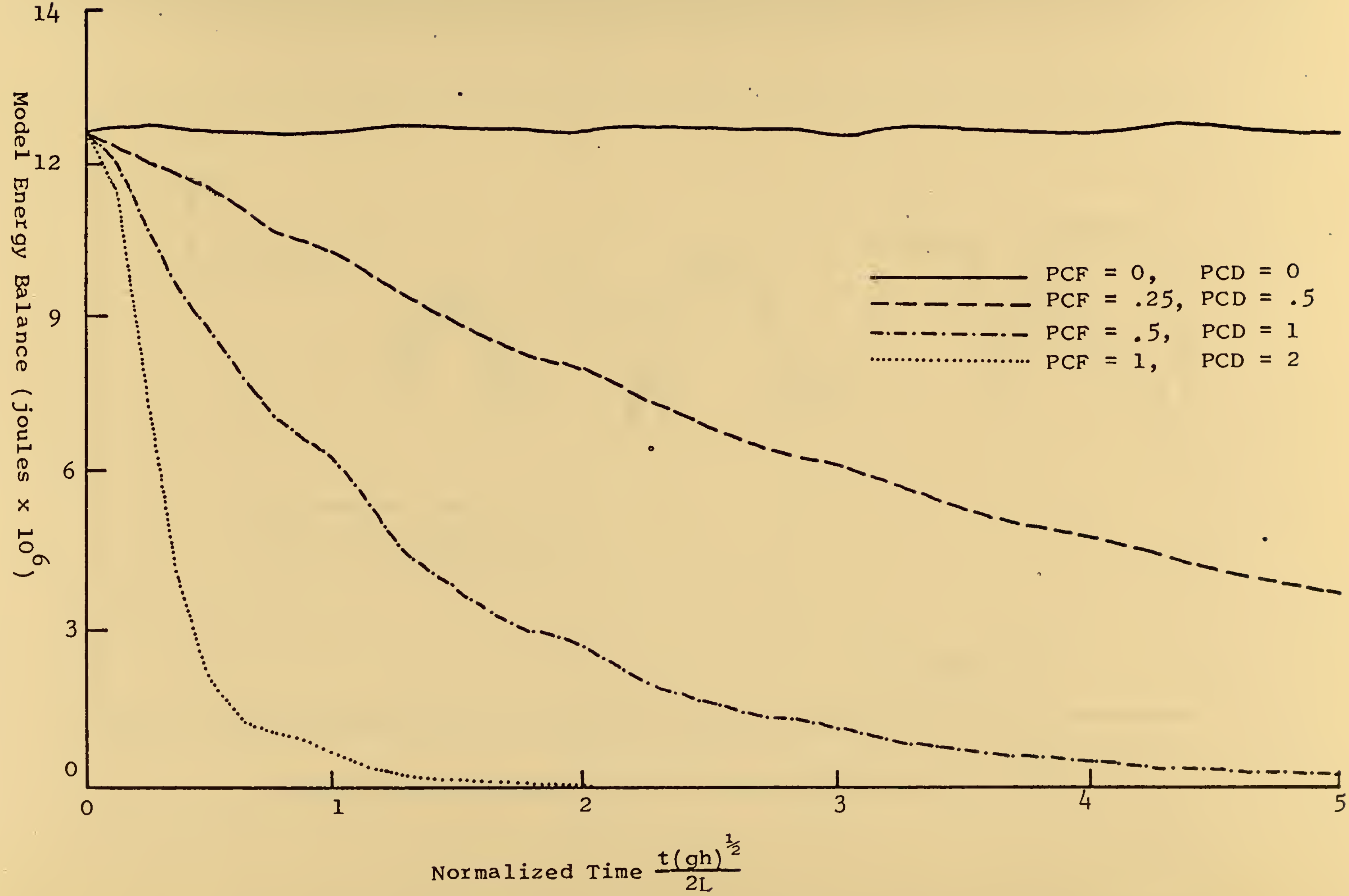

Figure 16. Effects of Inertial Rotation and Friction on Energy Balance.

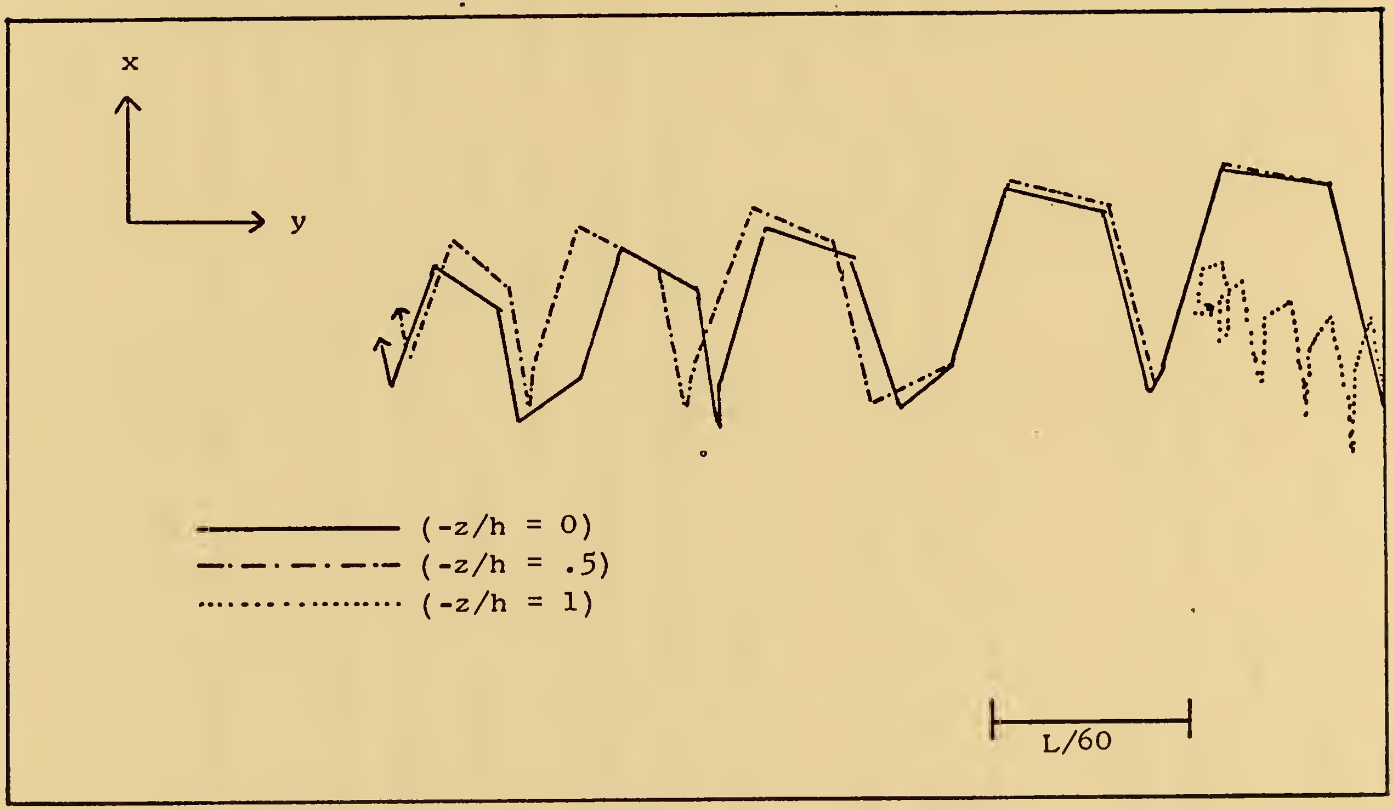

Figure 17. Hodograph of Mid-channel Velocity (t = 5T).

The rectification of the along channel flow was also a predominate characteristic of the flow where inertial rotation was considered. Figures 13 and 14 again show this relationship, as modified by friction, and Figure 15 depicts the combined effect on the free surface. It can be seen that for an extreme case (PCD = 1, PCF = 1) the free surface only very slowly slumps to a zero potential because friction retards the cross-channel flow long enough for rotation to reverse its direction before the free surface reaches the horizontal.

Figure 16 indicates that with rotation the energy level is damped with relatively fewer oscillations. It must be realized however that as (PCF) increases, the model is describing motion on an increasing time scale.

Figure 17 represents the path that would be taken by fluid particles (or suspended matter) at three levels in the column over five periods of oscillation. In addition to the rectification previously noted, there appears to be a net drift of the motion in the initial cross-channel transport direction. A closer examination of Figures 13 and 14 also show this drift and is a combined result of rotation and friction. Since the motion is being continuously damped by friction, the cross-channel transport can not return the fluid to its initial position after each oscillation and a net transport in the initial direction of motion results. The net drift is then strictly a function of initial set-up conditions of the free surface. The velocity profiles depicted in Figures 18 through 20 show some of the fine details of the flow with the combined influences of friction and inertial rotation.

Figure 18. Effects of Friction and Inertial Rotation on Mid-channel Velocity (PCF = 1, PCD = 1).

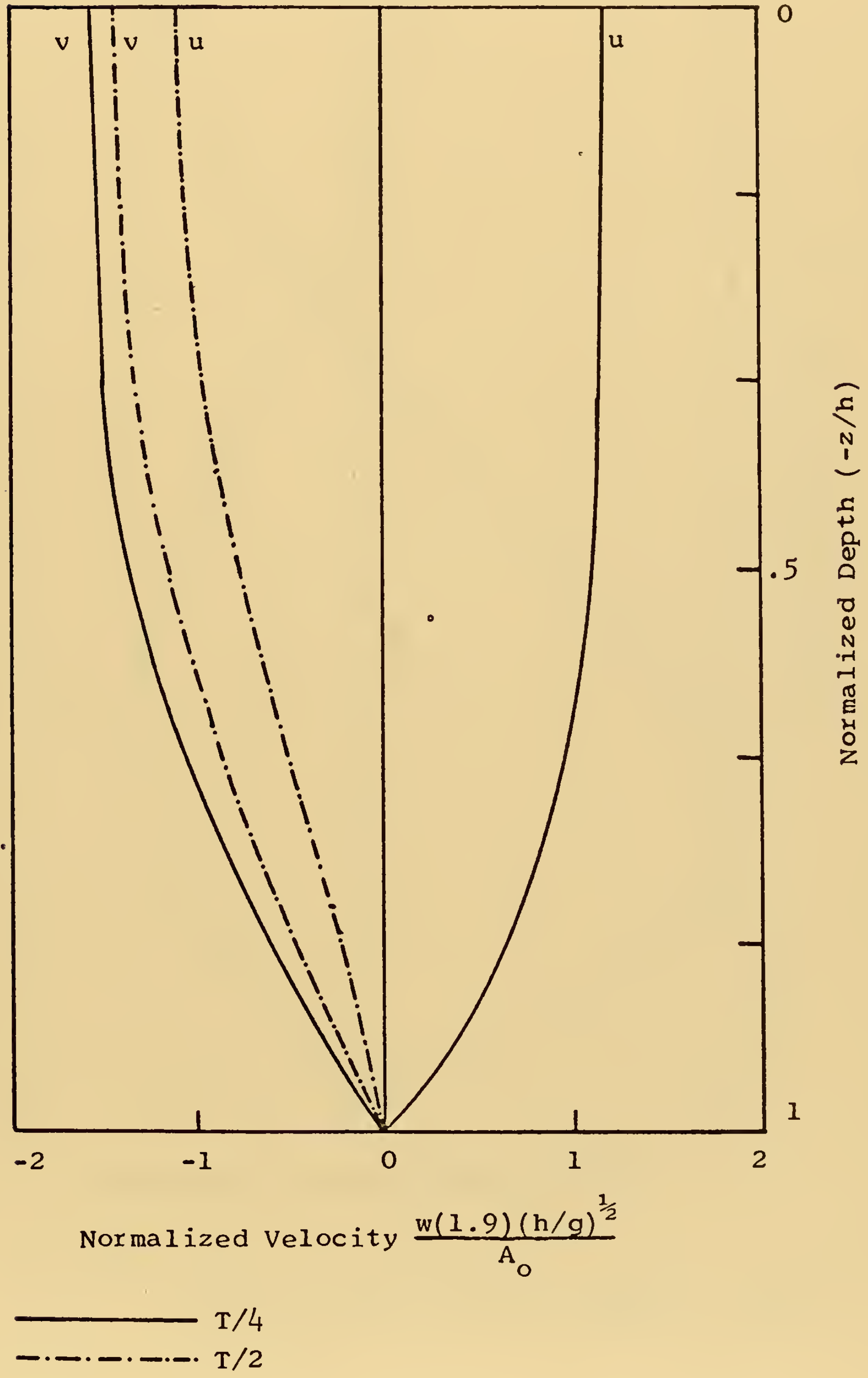

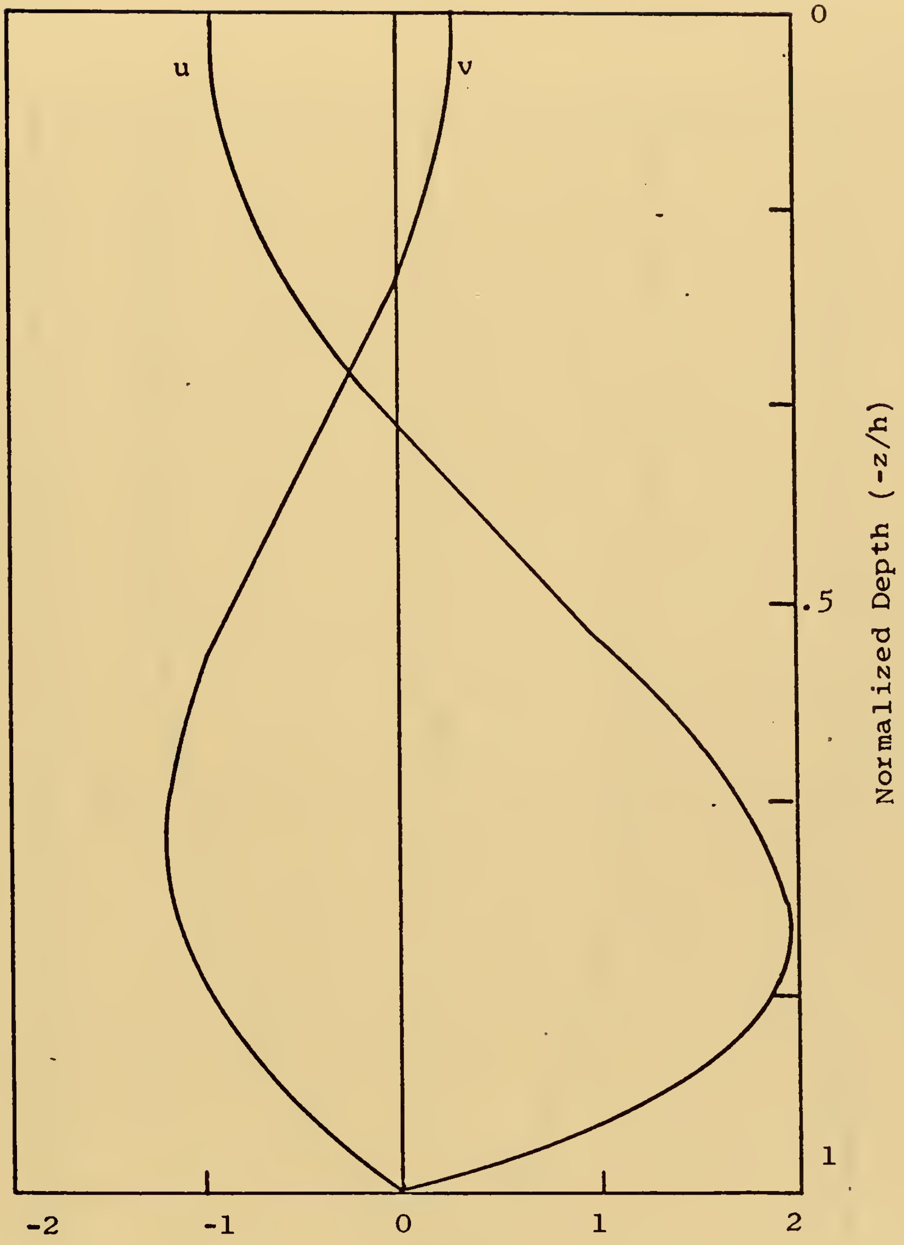

Normalized Velocity $\frac{w(11.4)(h/g)^{\frac{1}{2}}}{A_o}$

Figure 19. Effects of Friction and Inertial Rotation on Mid-channel Velocity (PCF = 1, PCD = 1, t = 3T/4).

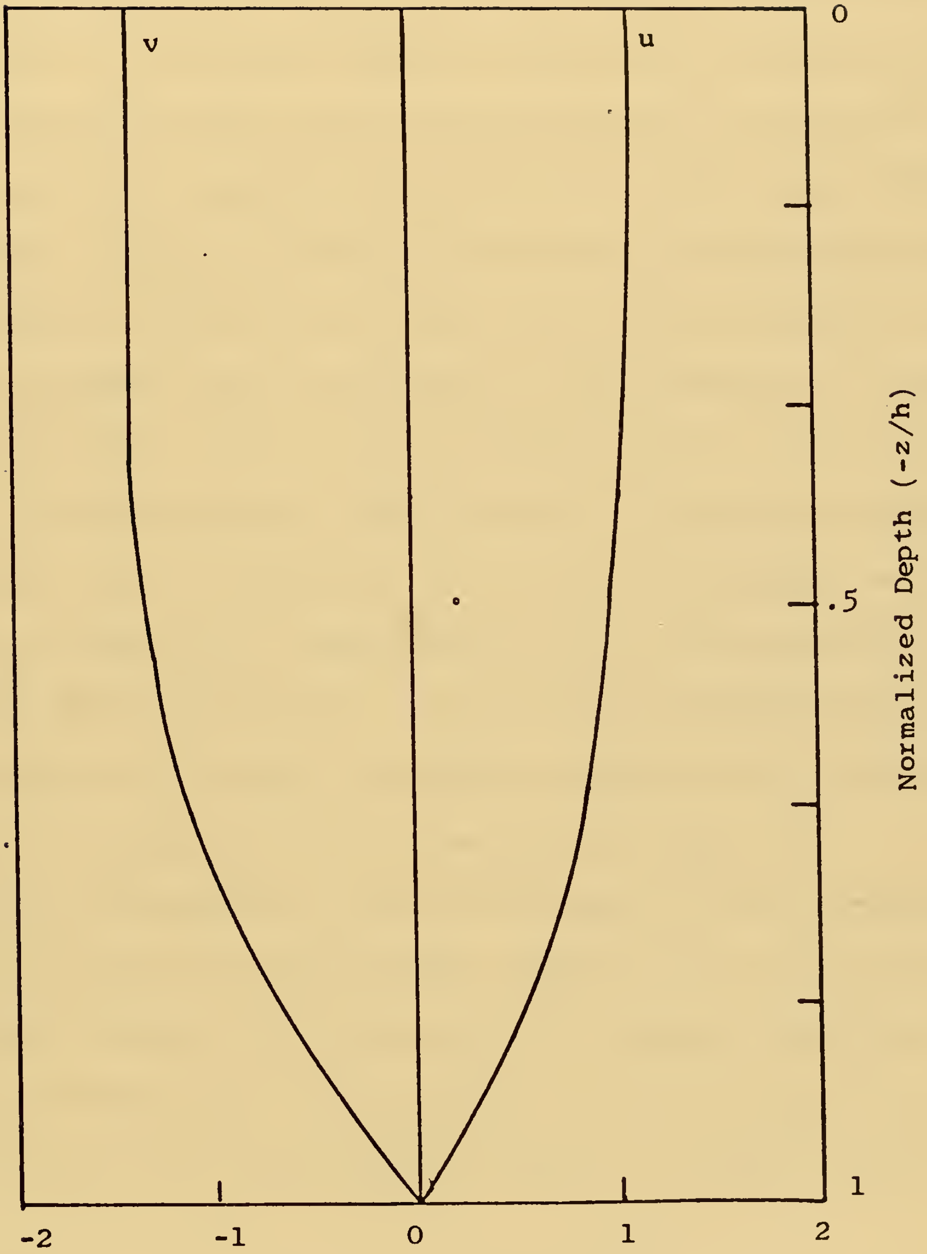

Normalized Velocity $\frac{w(2.86)(h/g)^{\frac{1}{2}}}{A_o}$

Figure 20. Effects of Friction and Inertial Rotation on Mid-channel Velocity (PCF = 1, PCD = 1, t = T).

The controlling influence on the stability of the water column continues to be the friction, however the interactions of the fluid are now more complicated due to the introduction of inertial rotation. Under the influence of increasing frictional dominance towards the bottom, the left rotation induced in the flow by Coriolis is increasingly damped, resulting in the familiar Ekman spiral. During periods of the motion previously described as smooth, the spiral remains fairly constant as the column rotates to the left. However, during the transition periods (Figure 19) when frictional influence is reduced due to decreasing flow velocity, the spiral unwinds from the bottom and varing amounts of twisting of the column results. This is again evidence of the transitional nature of the fluid during these periods. It should be noted that the velocity scale of Figure 19 is an order of magnitude smaller than that of Figure 18, indicating how small the velocities of the column are during transition. As the flow once again becomes uniform, the spiral is quickly re-established under the stabilizing influence of bottom friction, as depicted in Figure 20.

It is interesting to note from Figure 18 that during the transition periods the along channel component of velocity does in fact change direction for brief periods. Because these periods are of such short duration, this velocity reversal along the channel does not contribute to any significant transport, in this direction.

C. DISCUSSION OF THE GEOPHYSICAL SIMULATIONS

All of the previously discussed processes characteristic of time dependent motion, were observed during runs 26 through 30.

However, since the magnitude of these processes are Coriolis and frictional dependent, they occurred on a much smaller scale than observed for the test cases.

The model generated the time dependent variables produced by the seiche on a time scale equivalent to the resonance period of the basin. For these geophysical simulations, the periods were all too small to allow inertial rotation to have any significant effect on the motion. However, for shallow seas of large horizontal extent, values of (PCF) approaching .25 are entirely possible and test runs 1 through 4 showed that inertial effects would be significant and must be considered. Additionally, motion whose time scale is driven by external forces, independent of the resonance basin, are likely to be significantly altered by rotational dependence. For example the long period waves propagating up and down the continental shelf probably experience all the rotational characteristics associated with the time dependent motion described in the previous section. The observed phenomenon of transport rectification might occur in these systems and suggests a mechanism for modifying bed load transfer across the shelf. This process is a function of initial conditions and appears to require a period of static equilibrium just prior to initial motion. A region where the seasonal migration of atmospheric pressure systems are predominantly in one direction, might satisfy these requirements, with a resulting net rectification in one direction. Although this process is highly speculative, it certainly appears possible and a modification to the model to facilitate its study is suggested in Section V.

The frictional effects observed during runs 26 through 30 were also minimal. It should be noted that Ekman depths of greater than

20 meters are possible and thus these test runs represent a minimum frictional dependence.

The exception to these minimal effects was the observed phase lag between transport and bottom stress. This lag was pronounced in all cases and for the simulation of South San Francisco Bay, for example, averaged 40 degrees. This indicates that even small amounts of friction are important and re-emphasizes the need for a mathematical representation of time dependent transients that allows independent calculation of variables such as bottom stress and transport.

V. CONCLUSIONS AND RECOMMENDATIONS FOR FURTHER WORK

The model demonstrated that eq. (22) was a suitable mathematical representation of the time dependent motion described by the governing equations and the initial/boundary conditions. In this formulation the time dependent variables were uniquely determined by the local time histories of the surface at each point and this allowed independent representation of the various transients. The model further demonstrated the feasibility of developing a totally implicit finite-difference scheme for approximating eqs. (3) and (22) with acceptable accuracy. With the insight gained from the results it should be possible to improve the accuracy of the system by removing some of the important restrictions imposed by the Ekman dynamics and the simplified model.

The physical processes observed with time dependent motion showed the relative importance of friction and inertial rotation in determining the nature of the variables. It was apparent that for the larger time scales (PCF on the order of .25 or larger), Coriolis accelerations are important to the flow and must be considered. However, shorter time scales will probably be adequately represented neglecting rotation with little accuracy loss. During the data analysis it appeared that friction, even in small amounts, exerted considerable influence on the characteristics of the variables and their relationships, and should therefore not be neglected in representing time dependent motion.

Since frictional effects are predominant in the system, the simplified assumption of a constant coefficient of vertical friction throughout the layer, is probably one of the most limiting factors on the model's accuracy. A technique for improving the representation of the influence of friction might be the assumption of constant stress layer (Prandl layer) underlying the Ekman layer. The solutions in these layers would be matched at their interface; that is, at some height above the bottom determined as a function of the amount of friction present and the roughness of the bottom boundary. This method has been used in air-sea boundary layer models with considerable improvement in accuracy, and merits consideration at the ocean boundary in this scheme.

The assumption of constant depth does not account for modifications of the flow caused by changes in the potential vorticity induced by the shrinking and stretching of the water column over varying topography. This restriction is probably most serious in shallow regions where time dependent flow is significant and changes in the bottom extreme, for example the flow in the vicinity of the Monterey Submarine Canyon.

Certain large scale motions merit representation and investigation using this formulation. One of these is the study of seiches, especially the trapped modes, on the continental shelf since their buildup can cause storm surge (Pierson and Neuman, 1966). Also, as previously mentioned, the large scale oscillations on the continental shelf might make important contributions to sediment transfer across the shelf. Therefore it might prove useful to remove the horizontal boundary conditions from the model

and drive the flow by an externally specified time dependent forcing term. This would indicate how effectively the motion was coupled to these terms and show whether the previously noted transport rectification is of sufficient magnitude to be significant.

An examination of Tables I and II indicates how costly this type of numerical representation is in terms of computer time. It was not determined how much loss in resolution would occur by increasing the spacial grid size and reducing the length of the local time history considered. It is clear that considerable reduction in computing time would result and that such considerations are worth investigating before a similar model is used for extensive production runs.

APPENDIX A

DETAILS OF THE FINITE-DIFFERENCE SCHEME

Consider first the calculation of the components of the vector D_j, recalling that

$$D_j = \alpha\theta^n_{j+1} + \theta^n_j - \alpha\theta^n_{j-1} + \Delta tA \qquad (A1)$$

where

$$\alpha = \frac{\Delta t}{4\Delta x}\begin{vmatrix} 0 & 0 & C2/\Delta t \\ 0 & 0 & D2/\Delta t \\ -1 & 0 & 0 \end{vmatrix} \; ; \qquad (A2)$$

$$\theta^n_j = \begin{Bmatrix} U^n_j \\ V^n_j \\ \xi^n_j \end{Bmatrix} \; ; \qquad (A3)$$

$$A = \begin{Bmatrix} C1/\Delta t \\ D1/\Delta t \\ 0 \end{Bmatrix} \; ; \qquad (A4)$$

and

$$D_j = \begin{Bmatrix} d^j_1 \\ d^j_2 \\ d^j_3 \end{Bmatrix} \; ; \qquad (A5)$$

Expanding eq. (A1) using (A2) through (A4) yields:

$$D_j = \frac{\Delta t}{4\Delta x} \begin{vmatrix} 0 & 0 & C2/\Delta t \\ 0 & 0 & D2/\Delta t \\ -1 & 0 & 0 \end{vmatrix} \begin{Bmatrix} U_{j+1}^n \\ V_{j+1}^n \\ \xi_{j+1}^n \end{Bmatrix} + \begin{Bmatrix} U_j^n \\ V_j^n \\ \xi_j^n \end{Bmatrix}$$

$$- \frac{\Delta t}{4\Delta x} \begin{vmatrix} 0 & 0 & C2/\Delta t \\ 0 & 0 & D2/\Delta t \\ -1 & 0 & 0 \end{vmatrix} \begin{Bmatrix} U_{j-1}^n \\ V_{j-1}^n \\ \xi_{j-1}^n \end{Bmatrix} + \begin{Bmatrix} C1 \\ D1 \\ 0 \end{Bmatrix} \qquad (A6)$$

or,

$$D_j = \begin{Bmatrix} (C2/4\Delta x)(\xi_{j+1}^n - \xi_{j-1}^n) + U_j^n + C1 \\ (D2/4\Delta x)(\xi_{j+1}^n - \xi_{j-1}^n) + V_j^n + D1 \\ (-\Delta t/4\Delta x)(U_{j+1}^n - U_{j-1}^n) + \xi_j^n \end{Bmatrix} = \begin{Bmatrix} d_1^j \\ d_2^j \\ d_3^j \end{Bmatrix} \qquad (A7)$$

Now consider the calculation of the matrix

$$E_j = \begin{vmatrix} e_{11}^j & e_{12}^j & e_{13}^j \\ e_{21}^j & e_{22}^j & e_{23}^j \\ e_{31}^j & e_{32}^j & e_{33}^j \end{vmatrix} , \quad j \geqq 1 \qquad (A8)$$

Recall eq. (49) and express it in inverse form as

$$E_j = (I + \alpha E_{j-1})^{-1} \alpha, \quad j \geqq 1 \qquad (A9)$$

where I is the (3 X 3) identity matrix. Using the appropriate values for I, α, and E_{j-1}, it is easily showed that

$$(I + \alpha E_{j-1}) = \begin{vmatrix} \left(1 + \frac{C2e_{31}^{j-1}}{4\Delta x}\right) & \left(\frac{C2e_{32}^{j-1}}{4\Delta x}\right) & \left(\frac{C2e_{33}^{j-1}}{4\Delta x}\right) \\ \left(\frac{D2e_{31}^{j-1}}{4\Delta x}\right) & \left(1 + \frac{D2e_{32}^{j-1}}{4\Delta x}\right) & \left(\frac{D2e_{33}^{j-1}}{4\Delta x}\right) \\ \left(-\frac{\Delta te_{11}^{j-1}}{4\Delta x}\right) & \left(-\frac{\Delta te_{12}^{j-1}}{4\Delta x}\right) & \left(1 - \frac{\Delta te_{13}^{j-1}}{4\Delta x}\right) \end{vmatrix} = \gamma^{j-1} \tag{A10}$$

Therefore,

$$(I + \alpha E_{j-1})^{-1} = \frac{1}{\mathrm{DET}(\gamma^{j-1})} \, \mathrm{ADJ}(\gamma^{j-1}) \tag{A11}$$

Where $\mathrm{DET}(\gamma^{j-1})$ is the determinant of the matrix (γ^{j-1}) and $\mathrm{ADJ}(\gamma^{j-1})$ is its adjoint. The computation of eq. (A11) are extremely lengthy and are not included. The resulting product of applying eq. (A11) to eq. (A9) is as follows:

$$E_j = \frac{1}{\mathrm{DET}_{j-1}} \begin{bmatrix} \left(\frac{C2e_{33}^{j-1}}{4\Delta x}\right) & 0 & \left(\frac{C2}{\Delta t} - \frac{C2e_{13}^{j-1}}{4\Delta x}\right) \\ \left(\frac{D2e_{33}^{j-1}}{4\Delta x}\right) & 0 & \left(\frac{D2}{\Delta t} - \frac{D2e_{13}^{j-1}}{4\Delta x}\right) \\ -\left(1+\frac{C2e_{31}^{j-1}}{4\Delta x}\right) & 0 & \left(\frac{C2e_{11}^{j-1}}{4\Delta x}\right) \end{bmatrix}, \quad j \geq 1 \tag{A12}$$

where,

$$\mathrm{DET}_{j-1} = 1 - \frac{1}{4\Delta x}(\Delta te_{13}^{j-1} - C2e_{31}^{j-1}) + \frac{C2\Delta t}{(4\Delta x)^2}(e_{33}^{j-1}e_{11}^{j-1} - e_{31}^{j-1}e_{13}^{j-1}). \tag{A13}$$

This completes the calculations of the components of E_j. Finally consider the calculations of the components of the vector

$$F_j = \begin{Bmatrix} f_1^j \\ f_2^j \\ f_3^j \end{Bmatrix} \tag{A14}$$

Recall eq. (50) and express in its inverse form as

$$F_j = (I + \alpha E_{j-1})^{-1}(D_j - \alpha F_{j-1}), \; j \geq 1 \tag{A15}$$

Again the computations of eq. (A11) are involved and are not included. The results of applying eq. (A11) to (A15) are as follows:

$$F_j = \frac{1}{DET_{j-1}} \begin{pmatrix} \left(1 - \frac{\Delta t e_{13}^{j-1}}{4\Delta x}\right) Q1 - \left(\frac{C2 e_{33}^{j-1}}{4\Delta x}\right) Q3 \\[2ex] \left[\left(- \frac{D2 e_{31}^{j-1}}{4\Delta x} + \frac{D2 \Delta t (e_{31}^{j-1} e_{13}^{j-1} - e_{33}^{j-1} e_{11}^{j-1})}{(4\Delta x)^2}\right) Q1 \right. \\ + \left(1 + \frac{C2 e_{31}^{j-1}}{4\Delta x} - \frac{C2 \Delta t (e_{31}^{j-1} e_{13}^{j-1} - e_{33}^{j-1} e_{11}^{j-1})}{(4\Delta x)^2}\right) Q2 \\ \left. - \left(\frac{D2 e_{33}^{j-1}}{4\Delta x}\right) Q3 \right] \\[2ex] \left(\frac{\Delta t e_{11}^{j-1}}{4\Delta x}\right) Q1 + \left(1 + \frac{C2 e_{31}^{j-1}}{4\Delta x}\right) Q3 \end{pmatrix}, \; j \geq 1 \tag{A16}$$

where,

$$\begin{aligned} Q1 &= d_1^j - \frac{C2 f_3^{j-1}}{4\Delta x} \\ Q2 &= d_2^j - \frac{D2 f_3^{j-1}}{4\Delta x} \\ Q3 &= d_3^j \quad \frac{\Delta t f_1^{j-1}}{4\Delta x} \end{aligned} \tag{A17}$$

Note that the middle term of the vector F_j is the entire quantity in the brackets.

The implicit scheme for computing U, V, and ξ can now be constructed. Writing eq. (46) as

$$\theta_{j-1}^{n+1} = E_{j-1}\theta_j^{n+1} + F_{j-1} \tag{A18}$$

and substituting the quantities previously derived for E_{j-1} and F_{j-1} yields:

$$U_{j-1}^{n+1} = e_{11}^{j-1}U_j^{n+1} + e_{13}^{j-1}\,\xi_j^{n+1} + f_1^{j-1} \tag{A19}$$

$$V_{j-1}^{n+1} = e_{21}^{j-1}U_j^{n+1} + e_{23}^{j-1}\,\xi_j^{n+1} + f_2^{j-1} \tag{A20}$$

$$\xi_{j-1}^{n+1} = e_{31}^{j-1}U_j^{n+1} + e_{33}^{j-1}\,\xi_j^{n+1} + f_3^{j-1} \tag{A21}$$

Equations (A7), (A12), (A13), (A16), (A17), and (A19) through (A21) represent the expressions used to implicitly calculate values for θ_j^n at each grid point in the manner described in the text.

APPENDIX B

DETAILS OF REPRESENTING C1*, C2*, VELOCITY AND BOTTOM STRESS

Consider the representation of C1* by first noting that the limits of integration have the following meaning:

$t = 0$ represents the initial condition time.

$t = t$ represents the present time.

$t = t + \Delta t$ represents the time at which the value of the various variables are to be calculated.

The integration of eq. (48) was performed numerically by dividing the total time into small intervals (Δt) and evaluating $\frac{\partial \xi}{\partial x}(t')$ as a constant at the mid-point of each interval. This allowed C1* to be numerically represented as follows:

$$C1^{*I}_{L} = - \frac{-2g}{h} \sum_{M=1}^{MAXM} \frac{1}{p^2} \sum_{N=1}^{I-1} \left(\frac{\partial \xi}{\partial x}\right)_L^{N-\frac{1}{2}} \left[e^{-kp^2 \Delta t} e^{-if\Delta t} - 1\right]$$

$$\times \int_{(I-N)\Delta t}^{(I-1-N)\Delta t} - e^{-kp^2(t-t')} e^{-if(t-t')} dt' \qquad \text{(B1)}$$

With the further assumption that the effect of inertial rotation was constant in each interval, $e^{-if(t-t')}$ was approximated at the mid-point as $e^{-if(I-\frac{1}{2}-N)\Delta t}$ and treated as a constant. Analytical integration of the remaining integral resulted in eq. (51). To solve for C1 and D1 the following relation was used, and the real and imaginary terms collected.

$$e^{ift} = \cos(ft) - i \sin(ft) \qquad \text{(B2)}$$

This allowed C1 and D1 to be represented as

$$C1_L^I = A1 \sum_{M=1}^{MAXM} \frac{A2}{p^2} \sum_{N=1}^{I-1} A3 \Big[e^{-kp^2 \Delta t} \cos\{f(I+\tfrac{1}{2}-N)\Delta t\}$$

$$- \cos\{f(I-\tfrac{1}{2}-N)\Delta t\}\Big] A4 \tag{B3}$$

$$D1_L^I = A1 \sum_{M=1}^{MAXM} \frac{A2}{p^2} \sum_{N=1}^{I-1} A3 \Big[e^{-kp^2 \Delta t} \sin\{f(I+\tfrac{1}{2}-N)\Delta t\}$$

$$- \sin\{f(I-\tfrac{1}{2}-N)\Delta t\}\Big] A4 \tag{B4}$$

where

$$A1 = \frac{-2g}{h}$$

$$A2 = \frac{1}{kp^2}\left(1 - e^{-kp^2 \Delta t}\right)$$

$$A3 = \left(\frac{\partial \xi}{\partial x}\right)_L^{N-\frac{1}{2}}$$

$$A4 = e^{-kp^2 (I-1-N)\Delta t}$$

Using the same assumption regarding constant inertial rotation in each time interval, $C2^*$ readily reduced to eq. (52). Applying eq. (B2) to eq. (52) yields:

$$C2 = A1 \cos(\tfrac{1}{2} f \Delta t) \sum_{M=1}^{MAXM} \frac{A2}{p^2} \tag{B5}$$

$$D2 = - A1 \sin(\tfrac{1}{2} f \Delta t) \sum_{M=1}^{MAXM} \frac{A2}{p^2} \tag{B6}$$

Consider now the scheme formulated to recover the velocity profile. Since velocity was calculated at time t + Δt, eq. (26) was represented by:

$$w = \frac{2g}{h} \sum_{M=1}^{MAXM} \frac{(-1)^m \cos(pz)}{p} \left\{ \int_0^t e^{-kp^2(t+\Delta t-t')} e^{-if(t+\Delta t-t')} \frac{\partial \xi}{\partial x}(t')dt' \right.$$

$$\left. + \int_t^{t+\Delta t} e^{-kp^2(t+\Delta t-t')} e^{-if(t+\Delta t-t')} \frac{\partial \xi}{\partial x}(t')dt' \right\} \qquad (B7)$$

Applying the same assumptions and relations to eq. (B7) as were applied to eq. (B1) yields:

$$u_L^I = - A1 \sum_{M=1}^{MAXM} \frac{A5}{p} \left\{ A2 \sum_{N=1}^{I-1} A3 \left[e^{-kp^2 \Delta t} \cos\{f(I+\tfrac{1}{2}-N)\Delta t\} \right] A4 \right.$$

$$\left. + \cos(\tfrac{1}{2} f \Delta t)(A2)(A6) \right\} \qquad (B8)$$

$$v_L^I = - A1 \sum_{M=1}^{MAXM} \frac{A5}{p} \left\{ A2 \sum_{N=1}^{I-1} A3 \left[-e^{-kp^2 \Delta t} \sin\{f(I+\tfrac{1}{2}-N)\Delta t\} \right] A4 \right.$$

$$\left. - \sin(\tfrac{1}{2} f \Delta t)(A2)(A6) \right\} \qquad (B9)$$

where

$$A5 = (-1)^M \cos(pz)$$

$$A6 = \left(\frac{\partial \xi}{\partial x}\right)_L^{I-\frac{1}{2}}$$

The term (A5) represents the depth dependence and (A6) the slope in the most recent time interval. (A6) was calculated and stored by the model after U, V, and ξ were computed.

The final quantity needing representation is bottom stress (τ). Recalling eq. (54) and noting that the integral is identical to

that of eq. (26), bottom stress is easily represented as:

$$\begin{aligned}(\tau_x)_L^I = -\, kA1 \sum_{M=1}^{MAXM} \Big\{ & A2 \sum_{N=1}^{I-1} A3 \left[e^{-kp^2 \Delta t} \cos\{f(I+\tfrac{1}{2}-N)\Delta t\} \right] A4 \\ & + \cos(\tfrac{1}{2} f \Delta t)(A2)(A6) \Big\}\end{aligned} \tag{B10}$$

$$\begin{aligned}(\tau_y)_L^I = -\, kA1 \sum_{M=1}^{MAXM} \Big\{ & A2 \sum_{N=1}^{I-1} A3 \left[-e^{-kp^2 \Delta t} \sin\{f(I+\tfrac{1}{2}-N)\Delta t\} \right] A4 \\ & - \sin(\tfrac{1}{2} f \Delta t)(A2)(A6) \Big\}\end{aligned} \tag{B11}$$

Where (τ_x) and (τ_y) are cross-channel and along-channel components of stress respectively.

During the calculation of C1, D1, C2, D2, the model stores those common quantities needed for velocity and stress calculations as defined by eqs. (B3) through (B6), and (B8) through (B11). The program recalls these quantities and applies them to eqs. (B8) through (B11) whenever it is required to calculate velocity and bottom stress.

APPENDIX C

COMPUTER PROGRAM DESCRIPTION

The computer program was written in FORTRAN IV and was used with the IBM 360/67 computer system at the W.R. Church Computer Center, Naval Postgraduate School. The program has been generalized such that basin size, run time, initial free surface elevation, and number of modes considered in the solution can be varied in the data statements. Additionally, the model allows variable grid spacing, requiring only changes in the imput parameters and DIMENSION statements. The influence of inertial rotation and vertical friction are introduced into the model by the two non dimensional ratios discussed in the text.

FORTRAN IV symbols used for the major model parameters are defined below.

A	Model time (real time normalized to the free oscillating seiche period)
DH	Spacial step in depth (fixed at one meter)
DX	Spacial step in across-channel direction
DT	Time step
ETA	Free surface elevation
ETAX	Sea surface slope
ETAXS	Array for storing the time history of the sea surface slopes
F	Coriolis parameter
FREQ	Frequency of the free oscillating seiche

G	Acceleration of gravity
H	Depth of water
HI	Free surface elevation at left boundary
MAXH	Integer representation of water depth (must be even)
MAXL	Maximum number of cross-channel grid points (must be odd)
MAXP	Interval in time step when velocity, energy, and bottom stress is calculated
MAXT	Maximum number of time steps
PCD	Ratio of Ekman depth to depth of the water
PCF	Ratio of Coriolis parameter to depth of the water
PCT	Number of time steps per free wave period
PE	Potential energy of the seiche
PERD	Period of a free oscillating seiche
R	Coefficient of vertical friction
RHO	Density of the water
SE	Kinetic energy associated with the y-component of velocity
SIGMA	Angular frequency of a free oscillating seiche
STRESC	y-component of bottom stress
STRESR	x-component of bottom stress
T	Real time
TE	Kinetic energy associated with the x-component of velocity
TOT	Total energy balance of the seiche
UT	x-component of volume transport
VELC	y-component of velocity
VELR	x-component of velocity
VT	y-component of volume transport

The procedure for initialization of the program is as follows:

1) Modify the initial DATA statements to correspond to the parameters of the motion being represented.

2) Change DIMENSION statements accordingly.

3) Insure that appropriate storage and computer time requirements are satisfied. The program required a maximum of 100K BYTES storage on the IBM 360/67 system and variable CPU usage time as depicted in Tables I and II.

4) A minor modification to the program is necessary when frictionless motions are being represented. If (PCD = 0) or (PCF = 0), remove the following three expressions from the program.

```
K = (I-1) - 10.0/CC
IF(K.LE.0)K = 1
DO 40 J = K, IM1
```

Replace these expressions by

```
DO 40 J = 1, IM1
```

5) Because of the formulation, the program can not compute velocity at I = 1; therefore a value of MAXP = 1 should not be used. To recover the velocity profile at each time step ($I \neq 1$), initialize the DATA with MAXP = 2 and insert the statement (MAXP = 1) immediately before statement number 300.

The program, as appearing in the next section, is initialized in the MKS system and changes in the imput should be made accordingly. The major computational sections of the program are prefaced by appropriate comment statements, and a reader with FORTRAN IV experience should have little difficulty following the program.

COMPUTER PROGRAM

```
      DIMENSION ETA1(11),ETA2(11),ETAX(11),ETAX1(11),
     1ETAXS(11,201),UT1(11),UT2(11),VT1(11),VELR(11,31),
     2VELC(11,31),FUNR(11,25),FUNC(11,25),P(25),P2(25),
     3P3(25),P4(25),PK(25),B(31),C(31),TIN(11),PIN(11),
     4POT(11),E11(10),E21(10),E31(10),E13(10),E23(10),
     5E33(10),D1(10),D2(10),D3(10),F1(10),F2(10),F3(10),
     6DET(10),CR1(11),CC1(11),STRESR(11),STRESC(11)
C
C     INPUT INITIAL DATA
C
      DATA MAXT,MAXL,MAXH,MAXP,MAXM/200,11,30,5,25/
      DATA WIDTH,HI,PCT,DH,RHO/5000.,1.,40.,1.,1027./
      DATA PIE,G,PCF,PCD/3.1415927,9.8,.5,0.0/
C
C     ECHO CHECK DATA
      WRITE(6,310)
      WRITE(6,320)MAXT,MAXL,MAXH,MAXP,MAXM
      WRITE(6,330)WIDTH,HI,DH,RHO,PIE,G,PCT,PCF,PCD
C
      DX=WIDTH/FLOAT(MAXL-1)
      H=FLOAT(MAXH)
      PERD=(2.0*WIDTH)/SQRT(G*H)
      FREQ=1.0/PERD
      SIGMA=2.0*PIE*FREQ
      F=PCF*SIGMA
      R=(PCD*H)**2*F/(2.0*PIE**2)
      DT=PERD/PCT
      Q1=DT/(4.0*DX)
      Q2=4.0*DX
      C3=-2.0*G/H
      WRITE(6,350)H,WIDTH,DT,DX,PERD,SIGMA,F,R
C
C     COMPUTE AND STORE INITIAL CONDITIONS ON ETA,ETAX,UT,VT
C
      DO 10 L=1,MAXL
      X=(L-1)*DX
      ETA1(L)=HI*COS(PIE*X/WIDTH)
      ETAX(L)=(-1.0*PIE*HI/WIDTH)*SIN(PIE*X/WIDTH)
      UT1(L)=0.0
      VT1(L)=0.0
   10 CONTINUE
      A=0.0
      ETAX(MAXL)=0.0
C
C     PRINT INITIAL CONDITIONS
C
      WRITE(6,360)A
      WRITE(6,370)(ETA1(L),L=1,MAXL)
      WRITE(6,380)(ETAX(L),L=1,MAXL)
      WRITE(6,400)(UT1(L),L=1,MAXL)
      WRITE(6,405)(VT1(L),L=1,MAXL)
C
C     CALCULATE AND STORE MODAL CONSTANTS
C
      DO 20 M=1,MAXM
      P(M)=(2.0*FLOAT(M)-1.0)*PIE/(2.0*H)
      P2(M)=P(M)**2
      PK(M)=P2(M)*R
      P4(M)=EXP(-PK(M)*DT)
      C5=PK(M)
      C4=C5*DT
      IF(C4.LT.1.E-4)GO TO 15
      P3(M)=(1.0-EXP(-C4))/C5
      GO TO 20
   15 P3(M)=(DT*(1.0-(DT*C5/2.0)*(1.0-C5*DT/3.0)))
   20 CONTINUE
```

```
C
C     CALCULATE CR2 AND CC2
C
      FDT=F*DT
      C1=COS(.5*FDT)
      C2=SIN(.5*FDT)
      CR2=0.0
      DO 30 M=1,MAXM
      CR2=CR2+P3(M)/P2(M)
   30 CONTINUE
      CC2=-C3*C2*CR2
      CR2=C3*C1*CR2
C
C     BEGIN TIME LOOP
C
      DO 300 I=1,MAXT
      T=I*DT
      A=T/PERD
      IF(I.NE.1)GO TO 35
      DO 31 L=1,MAXL
      CR1(L)=0.0
      CC1(L)=0.0
   31 CONTINUE
C
C     SET LEFT BOUNDRY VALUES FOR MATRICES
C
      E11(1)=0.0
      E21(1)=0.0
      E31(1)=0.0
      E13(1)=0.0
      E23(1)=0.0
      E33(1)=1.0/.951
      F1(1)=0.0
      F2(1)=0.0
      F3(1)=0.0
      DET(1)=1.0
      GO TO 65
C
C     (I.NE.1) CALCULATE CR1 AND CC1
C
   35 DO 60 L=1,MAXL
      C6=0.0
      C7=0.0
      DO 50 M=1,MAXM
      FACR1=0.0
      FACR2=0.0
      FACC1=0.0
      FACC2=0.0
      CC=PK(M)*DT
      IM1=I-1
      K=(I-1)-10.0/CC
      IF(K.LE.0)K=1
      DO 40 J=K,IM1
      C4=ETAXS(L,J)
      C5=EXP(-CC*(I-1-J))
      FACR1=FACR1+C4*COS(FDT*(I+.5-J))*C5
      FACR2=FACR2-C4*COS(FDT*(I-.5-J))*C5
      FACC1=FACC1-C4*SIN(FDT*(I+.5-J))*C5
      FACC2=FACC2+C4*SIN(FDT*(I-.5-J))*C5
   40 CONTINUE
      FACR1=FACR1*P4(M)
      FACC1=FACC1*P4(M)
      C5=P3(M)
      FUNR(L,M)=FACR1*C5
      FUNC(L,M)=FACC1*C5
      C8=1.0/P2(M)
      C6=C6+(FACR1+FACR2)*C5*C8
      C7=C7+(FACC1+FACC2)*C5*C8
   50 CONTINUE
      CR1(L)=C3*C6
      CC1(L)=C3*C7
   60 CONTINUE
```

```
C
C     CALCULATE VALUES OF MATRICIES
C
   65 MM1=MAXL-1
      DO 70 L=2,MM1
      D1(L)=(CR2/Q2)*(ETA1(L+1)-ETA1(L-1))+UT1(L)+CR1(L)
      D2(L)=(CC2/Q2)*(ETA1(L+1)-ETA1(L-1))+VT1(L)+CC1(L)
      D3(L)=-Q1*(UT1(L+1)-UT1(L-1))+ETA1(L)
      Q3=Q1/DET(L-1)
      E11(L)=Q3*CR2*E33(L-1)/Q2
      E13(L)=Q3*(CR2/DT-CR2*E13(L-1)/Q2)
      E21(L)=Q3*CC2*E33(L-1)/Q2
      E23(L)=Q3*(CC2/DT-CC2*E13(L-1)/Q2)
      E31(L)=-Q3*(1.0+CR2*E31(L-1)/Q2)
      E33(L)=Q3*CR2*E11(L-1)/Q2
      DET(L)=1.0-(1.0/Q2)*(DT*E13(L)-CR2*E31(L))+(CR2*DT/Q2
     1**2)*(E33(L)*E11(L)-E31(L)*E13(L))
      Q4=D1(L)-CR2*F3(L-1)/Q2
      Q5=D2(L)-CC2*F3(L-1)/Q2
      Q6=D3(L)+DT*F1(L-1)/Q2
      F1(L)=((1.0-DT*E13(L-1)/Q2)*Q4-(CR2*E33(L-1)/Q2)*Q6)/
     1DET(L-1)
      C4=(-CC2*E31(L-1)/Q2+CC2*DT*(E31(L-1)*E13(L-1)-
     1E33(L-1)*E11(L-1))/Q2**2)*Q4
      C5=(1.0+(CR2*E31(L-1)-DT*E13(L-1))/Q2-CR2*DT*(E31(L-1)
     1*E13(L-1)-E33(L-1)*E11(L-1))/Q2**2)*Q5
      C6=(CC2*E33(L-1)/Q2)*Q6
      F2(L)=(C4+C5-C6)/DET(L-1)
      F3(L)=((DT*E11(L-1)/Q2)*Q4+(1.0+CR2*E31(L-1)/Q2)*Q6)/
     1DET(L-1)
   70 CONTINUE
C
C     COMPUTE UT2, VT1. ETA2
C
      ETA2(MM1)=F3(MM1)/(1.0-E33(MM1)/.951)
      ETA2(MAXL)=ETA2(MM1)/.951
      UT2(MM1)=E13(MM1)*ETA2(MAXL)+F1(MM1)
      VT1(MM1)=E23(MM1)*ETA2(MAXL)+F2(MM1)
      UT2(MAXL)=0.0
      VT1(MAXL)=0.0
      MM3=MAXL-3
      DO 80 L=1,MM3
      M=MAXL-L
      C4=UT2(M)
      C5=ETA2(M)
      ETA2(M-1)=E31(M-1)*C4+E33(M-1)*C5+F3(M-1)
      UT2(M-1)=E11(M-1)*C4+E13(M-1)*C5+F1(M-1)
      VT1(M-1)=E21(M-1)*C4+E23(M-1)*C5+F2(M-1)
   80 CONTINUE
      ETA2(1)=ETA2(2)/.951
      UT2(1)=0.0
      VT1(1)=0.0
C
C     COMPUTE ETAX1
C
      DO 85 L=2,MM1
      ETAX1(L)=(ETA2(L+1)-ETA2(L-1))/(2.0*DX)
   85 CONTINUE
      ETAX1(1)=0.0
      ETAX1(MAXL)=0.0
C
C     RESET ETAXS ARRAY AND RESET ETA1, ETAX, AND UT1
C
      DO 90 L=1,MAXL
      ETAXS(L,I)=(ETAX1(L)+ETAX(L))/2.0
      UT1(L)=UT2(L)
      ETA1(L)=ETA2(L)
      ETAX(L)=ETAX1(L)
   90 CONTINUE
C
C     PRINT OUT UT1, VT1. ETA1. AND ETAX
C
```

```
      WRITE(6,410)A
      WRITE(6,420)(UT1(L),L=1,MAXL)
      WRITE(6,421)(VT1(L),L=1,MAXL)
      WRITE(6,425)(ETA1(L),L=1,MAXL)
      WRITE(6,429)(ETAX(L),L=1,MAXL)
C
      IF(MOD(I,MAXP).EQ.0)GO TO 100
      GO TO 300
C
C     I IS A MULTIPLE OF MAXP, CALCULATE VELOCITY
C
  100 DO 115 L=1,MAXL
      C6=ETAXS(L,I)
      DO 110 M=1,MAXM
      FUNR(L,M)=FUNR(L,M)+C1*P3(M)*C6
      FUNC(L,M)=FUNC(L,M)-C2*P3(M)*C6
  110 CONTINUE
  115 CONTINUE
      DO 140 L=1,MAXL
      MH1=MAXH+1
      DO 130 J=1,MH1
      Z=(J-1)*DH
      SI=-1.0
      C4=0.0
      C5=0.0
      DO 120 M=1,MAXM
      C6=P(M)
      C7=COS(C6*Z)/C6
      C4=C4+SI*FUNR(L,M)*C7
      C5=C5+SI*FUNC(L,M)*C7
      SI=-1.0*SI
  120 CONTINUE
      VELR(L,J)=-C3*C4
      VELC(L,J)=-C3*C5
  130 CONTINUE
  140 CONTINUE
C
C     CALCULATE BOTTOM STRESS
C
      C6=C3*R
      DO 142 L=1,MAXL
      C4=0.0
      C5=0.0
      DO 141 M=1,MAXM
      C4=C4+FUNR(L,M)
      C5=C5+FUNC(L,M)
  141 CONTINUE
      STRESR(L)=C4*C6
      STRESC(L)=C5*C6
  142 CONTINUE
C
C     CALCULATE ENERGY BALANCE USING SIMPSON'S RULE
C
  145 DO 165 L=1,MAXL
      DO 150 J=1,MH1
      B(J)=VELR(L,J)**2
      C(J)=VELC(L,J)**2
  150 CONTINUE
      EVSUM1=0.0
      EVSUM2=0.0
      ODSUM1=0.0
      ODSUM2=0.0
      ENSUM1=B(1)+B(MH1)
      ENSUM2=C(1)+C(MH1)
      MH2=MH1-1
      DO 155 J=2,MH2,2
      EVSUM1=EVSUM1+B(J)
      EVSUM2=EVSUM2+C(J)
  155 CONTINUE
      MH2=MH1-2
      DO 160 J=3,MH2,2
      ODSUM1=ODSUM1+B(J)
```

```
      ODSUM2=ODSUM2+C(J)
  160 CONTINUE
      TIN(L)=DH/3.0*(ENSUM1+2.0*ODSUM1+4.0*EVSUM1)
      PIN(L)=DH/3.0*(ENSUM2+2.0*ODSUM2+4.0*EVSUM2)
      POT(L)=ETA1(L)**2
  165 CONTINUE
      EVSUM1=0.0
      EVSUM2=0.0
      EVSUM3=0.0
      ODSUM1=0.0
      ODSUM2=0.0
      ODSUM3=0.0
      ENSUM1=POT(1)+POT(MAXL)
      ENSUM2=TIN(1)+TIN(MAXL)
      ENSUM3=PIN(1)+PIN(MAXL)
      DO 170 L=2,MM1,2
      EVSUM1=EVSUM1+POT(L)
      EVSUM2=EVSUM2+TIN(L)
      EVSUM3=EVSUM3+PIN(L)
  170 CONTINUE
      MM2=MAXL-2
      DO 175 L=3,MM2,2
      ODSUM1=ODSUM1+POT(L)
      ODSUM2=ODSUM2+TIN(L)
      ODSUM3=ODSUM3+PIN(L)
  175 CONTINUE
      PE=.5*RHO*G*(DX/3.0)*(ENSUM1+ 2.0*ODSUM1+4.0*EVSUM1)
      TE=.5*RHO*(DX/3.0)*(ENSUM2+2.0*ODSUM2+4.0*EVSUM2)
      SE=.5*RHO*(DX/3.0)*(ENSUM3+2.0*ODSUM3+4.0*EVSUM3)
      TOT=PE+TE+SE
C
C     PRINT VELOCITY
C
      WRITE(6,430)
      DO 180 J=1,MH1
      JM1=J-1
      WRITE(6,440)JM1,(VELR(L,J),L=1,MAXL)
  180 CONTINUE
      WRITE(6,435)
      DO 190 J=1,MH1
      JM1=J-1
      WRITE(6,440)JM1,(VELC(L,J),L=1,MAXL)
  190 CONTINUE
C
C     PRINT PE,TE,SE,TOT,STRESR, AND STRESC
C
      WRITE(6,450)PE,TE,SE,TOT
      WRITE(6,455)(STRESR(L),L=1,MAXL)
      WRITE(6,460)(STRESC(L),L=1,MAXL)
C
  300 CONTINUE
C
      STOP
  310 FORMAT('1','ECHO CHECK OF INPUT DATA',/)
  320 FORMAT('0',5I4)
  330 FORMAT('0',9E11.3)
  350 FORMAT('1','SOLUTION TO SEICHE PROBLEM WITH CORIOLIS',
     1'FOLLOWS',/,1X,'DEPTH=',F5.1,1X,'METERS',/,1X,
     2'WIDTH=',F7.1,1X,'METERS',/,1X,'DT=',F5.1,1X,'SEC',/,
     31X,'DX=',F6.1,1X,'METERS',/,1X,'PERD=',F7.1,1X,'SEC',
     4/,1X,'SIGMA=',E11.3,/,1X,'F=',E11.3,/,1X,'R=',E11.3,//
  360 FORMAT(' ',55X,'INITIAL CONDITIONS',/,56X,'TIME=',
     1F4.1,1X,'SECONDS')
  370 FORMAT(' ',55X,'ETA'/(11E11.3))
  380 FORMAT(' ',55X,'ETAX'/(11E11.3))
  400 FORMAT(' ',55X,'TRANSPORT(UT)'/(11E11.3))
  405 FORMAT(' ',55X,'TRANSPORT(VT)'/(11E11.3))
  410 FORMAT('0',55X,'NORMALIZED TIME=',F8.2,/)
  420 FORMAT(' ',55X,'TRANSPORT(UT)'/(11E11.3))
  421 FORMAT(' ',55X,'TRANSPORT(VT)'/(11E11.3))
  425 FORMAT(' ',55X,'ETA'/(11E11.3))
  429 FORMAT(' ',55X,'ETAX'/(11E11.3))
```

```
430  FORMAT('0',55X,'VELOCITY(VELR)',/,3X,'Z',/)
435  FORMAT('0',55X,'VELOCITY(VELC)',/,3X,'Z',/)
440  FORMAT(' ',2X,I2,(11E11.3))
450  FORMAT('0','PE=',2X,E15.7,8X,'TE=',E15.7,8X,'SE=',
    1E15.7,8X,'TOT=',E15.7)
455  FORMAT('0',55X,'STRESS(R)',/(11E11.3))
460  FORMAT('0',55X,'STRESS(C)',/(11E11.3))
     END
```

BIBLIOGRAPHY

Bryan, K., "A Numerical Investigation of Certain Features of the General Circulation," Tellus, v. 11, no. 2, p. 163-174, March, 1959.

Galt, J.A., "Linear Transients Associated with a Time Dependent Wind Over Shallow Water," Unpublished Paper, Naval Postgraduate School, 14 pp., 1970.

Hamming, R.G., Numerical Methods for Scientists and Engineers, McGraw-Hill, 1962.

McCalla, T.R., Introduction to Numerical Methods and FORTRAN Programming, p. 270-271, Wiley and Sons, 1967.

Morton, K.W. and Richtmyer, R.D., Difference Methods for Initial-Value Problems, p. 198-201, Interscience, 1957.

Munk, W.H., "On the Wind-Driven Ocean Circulation," Jour. of Meterology, v. 7, no. 2, p. 79-93, 1950.

Neuman, G. and Pierson, W.J., Principles of Physical Oceanography, p. 374-375, Prentice-Hall, 1966.

Proudman, J., Dynamical Oceanography, p. 243-245, Dover, 1952.

Smith, G.D., Numerical Solution of Partial Differential Equations, p. 70-71, Oxford University, 1965.

Sverdrup, H.U., "Wind-Driven Currents in a Baraclinic Ocean; with Application to the Equatorial Currents of the Eastern Pacific," Proc. Nat. Acad. Sci., v. 33, no. 11, p. 318-326, 1947.

Sverdrup, H.U., Johnson, M.W., and Fleming, R.H., The Oceans, pp. 1087, Prentice-Hall, 1942.

Welander, P., "Wind Action over Shallow Sea: Some Generalizations of Ekman's Theory," Tellus, v. 9, no. 1, p. 45-52, 1957.

Welander, P., "Numerical Prediction of Storm Surges," Adv. in Geogpy., v. 8, p. 315-379, 1961.

INITIAL DISTRIBUTION LIST

		No. Copies
1.	Defense Documentation Center Cameron Station Alexandria, Virginia 22314	2
2.	Library, Code 0212 Naval Postgraduate School Monterey, California 93940	2
3.	Department of Oceanography Naval Postgraduate School Monterey, California 93940	3
4.	Oceanographer of the Navy The Madison Building 732 N. Washington Street Alexandria, Virginia 22314	1
5.	Dr. Ned A. Ostenso Code 480D Office of Naval Research Arlington, Virginia 22217	1
6.	Asst. Prof. J.A. Galt, Code 58Gl Department of Oceanography Naval Postgraduate School Monterey, California 93940	4
7.	Asst. Prof. J.J. vonSchwind, Code 58Vs Department of Oceanography Naval Postgraduate School Monterey, California 93940	1
8.	Asst. Prof. K.L. Davidson, Code 51Ds Department of Meterology Naval Postgraduate School Monterey, California 93940	1
9.	Asst. Prof. R.H. Franke, Code 53 Fe Department of Mathematics Naval Postgraduate School Monterey, California 93940	1
10.	Asst. Prof. R.S. Andrews, Code 58Ad Department of Oceanography Naval Postgraduate School Monterey, California 93940	1
11.	LCDR Norman T. Camp, USN USS OPPORTUNE (ARS 41) FPO, New York, N.Y. 09501	1

DOCUMENT CONTROL DATA - R & D

(Security classification of title, body of abstract and indexing annotation must be entered when the overall report is classified)

1. ORIGINATING ACTIVITY *(Corporate author)* Naval Postgraduate School Monterey, California 93940	2a. REPORT SECURITY CLASSIFICATION Unclassified 2b. GROUP

3. REPORT TITLE
An Investigation of Linear Transients Associated With a Time Dependent Bottom Spiral

4. DESCRIPTIVE NOTES *(Type of report and, inclusive dates)*
Master's Thesis; March 1972

5. AUTHOR(S) *(First name, middle initial, last name)*
Norman Thomas Camp

6. REPORT DATE March 1972	7a. TOTAL NO. OF PAGES 93	7b. NO. OF REFS 13

8a. CONTRACT OR GRANT NO.	9a. ORIGINATOR'S REPORT NUMBER(S)
b. PROJECT NO.	
c.	9b. OTHER REPORT NO(S) *(Any other numbers that may be assigned this report)*
d.	

10. DISTRIBUTION STATEMENT

Approved for public release; distribution unlimited.

11. SUPPLEMENTARY NOTES	12. SPONSORING MILITARY ACTIVITY Naval Postgraduate School Monterey, California 93940

13. ABSTRACT

Ekman's linear equations for time dependent flow (neglecting wind stress) are solved using a time dependent Green's function and the method suggested by Welander (1957). The solution represents the vertical velocity profile in terms of the local time history of the changes in sea surface elevation determined by the divergence of the flow in the vertically integrated continuity equation.

A fully implicit finite-difference scheme is developed to represent a time dependent seiche oscillating across a shallow infinite channel. The transients associated with the formation of the bottom spiral are clearly represented by the model and the influence of friction and Coriolis are individually and collectively introduced. The model allows independent calculation of velocity, volume transport, sea surface elevation, bottom stress, and the total energy balance of the system. The numerical scheme provides a method for adequately describing and investigating certain classes of time dependent motion, and its development suggests a mechanism for improving numerical prediction of storm surge.

14. KEY WORDS	LINK A		LINK B		LINK C	
	ROLE	WT	ROLE	WT	ROLE	WT
Ekman dynamics						
Numerical model						
Seiche						
Shallow water flow						
Storm surge						
Time dependent motion						

DD FORM 1 NOV 65 1473 (BACK)
S/N 0101-807-6821

A-31409

Camp

An investigation of linear transients associated with a time dependent bottom spiral.

Thesis
C1932
c.1

Camp

134471

An investigation of linear transients associated with a time dependent bottom spiral.